


# Reduce electrical overload via threaded Chinese acupuncture in nerve electrical therapy

Yupu Liu<sup>1</sup>, Yawei Du<sup>1</sup> , Juan Wang<sup>1</sup>, Longxi Wu, Feng Lin, Wenguo Cui<sup>\*</sup>

Department of Orthopaedics, Shanghai Key Laboratory for Prevention and Treatment of Bone and Joint Diseases, Shanghai Institute of Traumatology and Orthopaedics, Ruijin Hospital, Shanghai Jiao Tong University School of Medicine, 197 Ruijin 2nd Road, Shanghai, 200025, PR China

## ARTICLE INFO

### Keywords:

Bioelectrical stimulation  
Electrical overload  
Threaded microneedle electrode system  
Microspheres  
Neuroregeneration

## ABSTRACT

Bioelectrical stimulation is a powerful technique used to promote tissue regeneration, but it can be hindered by an “electrical overload” phenomenon in the core region of stimulation. We develop a threaded microneedle electrode system that protects against “electrical overload” by delivering medicinal hydrogel microspheres into the core regions. The threaded needle body is coated with polydopamine and chitosan to enhance the adhesion of microspheres, which are loaded into the threaded grooves, allowing for their stereoscopic release in the core regions. After the electrode is inserted, the microspheres can be delivered three-dimensionally through physical swelling and the shear-thinning effect of chitosan, mitigating the electrical damage. Microspheres are designed to release alkylated vitamin B12 and vitamin E, providing antioxidant and cell protection effects upon *in-situ* activation, reducing reactive oxygen species (ROS) by 72.8 % and cell death by 59.5 %. In the model of peripheral nerve injury, the electrode system improves the overall antioxidant capacity by 78.5 % and protects the surrounding cells. Additionally, it leads to an improved nerve conduction velocity ratio of 41.9 % and sciatic nerve function index of 12.1 %, indicating enhanced neuroregeneration. The threaded microneedle electrode system offers a promising approach for nerve repair by inhibiting “electrical overload”, potentially improving outcomes for tissue regeneration.

## 1. Introduction

Bioelectrical stimulation has become widely used in the therapeutic management of various medical conditions, including nerve injuries [1], muscle atrophy [2], and pain relief [3]. However, electrical stimulation has a wide range of effects, and some mechanisms may be negative; there is a lack of research in this area, and screening out the negative mechanisms may be more conducive to improving electrical stimulation and enhancing efficacy. Here, the phenomenon termed “electrical overload” in the core region can lead to cell damage and poor treatment outcomes. Unless the electrodes are infinite, there is bound to be a difference in current distribution density [4]. Due to differences in human tissues, attenuation of the signal in muscle tissue and scattering at bone are more likely to occur [5]. Due to tissue heterogeneity, there are also effects on the level of stimulation considered safe and does not induce axonal damage [6]. This issue, often overlooked in biostimulation applications, arises due to the inherent impedance of tissues and extracellular matrices [7–9].

In the electrode core region, electric field potential increases to maintain adequate potential in intermediate areas, leading to concentrations of “electrical overload” [10]. This heightened electric field potential can elevate cell membrane permeability, disrupt osmotic balance, alter ion channel states, and impact cellular metabolism and ion distribution. Additionally, after tissue damage, applying electrical stimulation can further modify current distribution in the core region, possibly resulting in additional harm [11]. Moreover, electrolytic byproducts like hydrogen peroxide, hydroxyl radicals, and superoxide radicals may contribute to oxidative stress and inflammatory responses, adversely affecting local cell and tissue regeneration [12]. While mechanisms of “electrical overload” have been studied in tumor therapy, their detrimental effects within regenerative medicine have not received sufficient attention [13]. Although reducing the intensity of electrical stimulation might mitigate the risks associated with “electrical overload”, this approach could also diminish treatment effectiveness. In clinical practice, repeated stimulation with increased current intensity is often employed to enhance therapeutic outcomes, which may

<sup>\*</sup> Corresponding author.

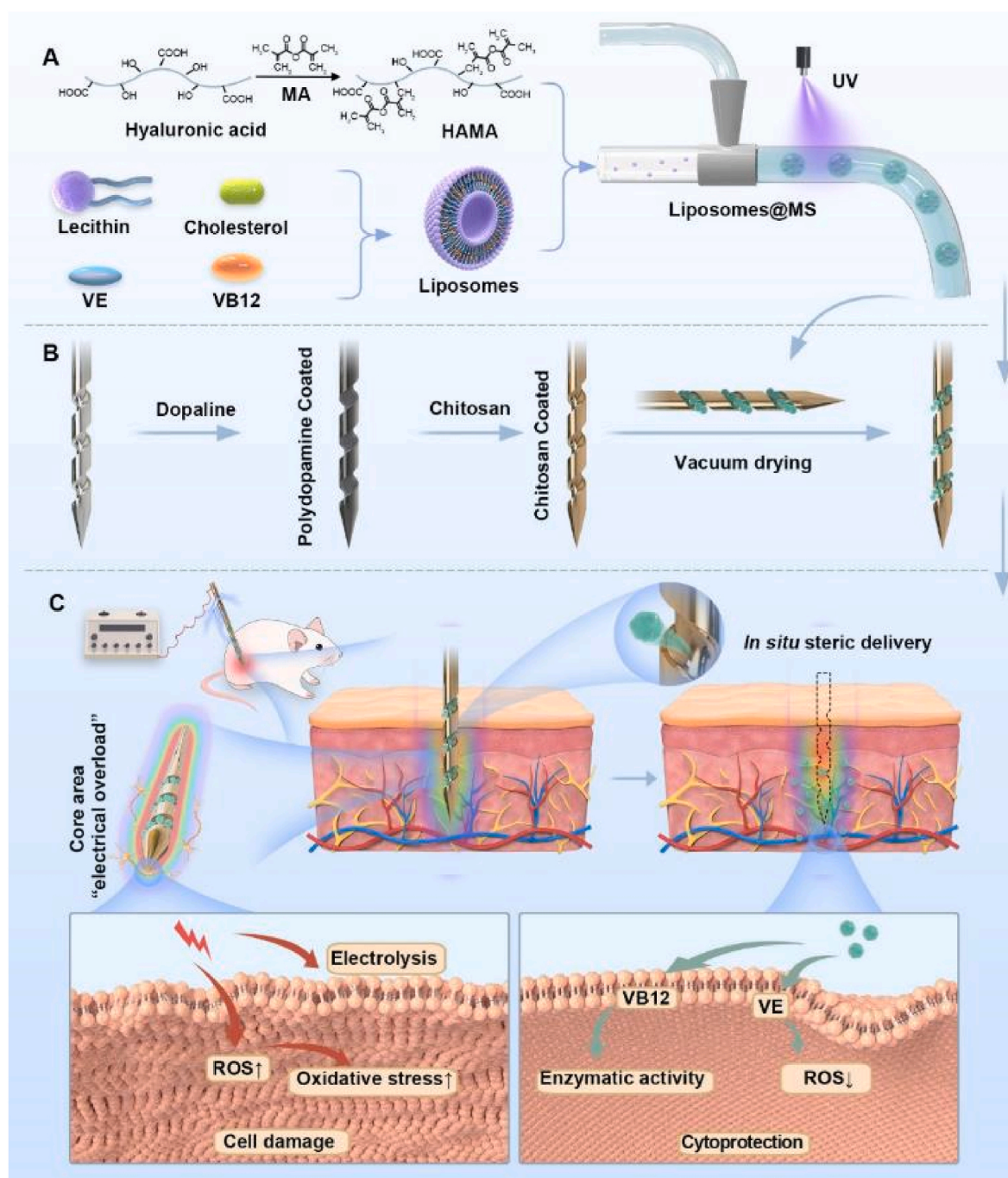
E-mail address: [wgcui@sjtu.edu.cn](mailto:wgcui@sjtu.edu.cn) (W. Cui).

<sup>1</sup> The authors contributed equally to this work.

inadvertently worsen “electrical overload” in the core region [14]. Therefore, it is essential to explore strategies that alleviate “electrical overload” while maintaining the efficacy of electrical stimulation in therapeutic applications.

To tackle the challenge of “electrical overload”, a critical approach involves achieving synchronized and precise drug delivery to the core area affected by electrical stimulation. However, local drug injections present certain challenges in counteracting “electrical overload”. Firstly, the injection site may not perfectly align with the area experiencing electrical stimulation. Secondly, the impact of electrical stimulation on local tissues is inherently three-dimensional. Furthermore, repetitive

electrical stimulation therapies necessitate multiple injections, which can lead to secondary trauma and further tissue damage, thereby decreasing patient acceptance and compliance [15]. Consequently, even localized injections struggle to concentrate drugs precisely in the core area of stimulation. To address these issues, developing a localized drug delivery strategy integrated with the electrode itself represents a promising research direction that aligns more closely with clinical needs. Among various electrode types, needle electrodes stand out as minimally invasive options inspired by traditional Chinese acupuncture needles, recognized for their high safety profile [16]. Due to their micrometer-sized elongated structure, needle electrodes possess a



**Scheme 1.** Threaded microneedle electrode systems alleviate “electrical overload”. (A) Preparation of HAMA microspheres loaded with VB12 and VE succinate using microfluidics. (B) Adhesion of microspheres to the grooves of the needle body using polydopamine and chitosan codeposited coatings, followed by vacuum drying. (C) When a threaded microneedle electrode system is used for electrical stimulation, the *in-situ* detachment of microspheres releases liposomes to deliver drugs to cells, thus alleviating the damage caused by “electrical overload” near the electrode.

smaller stimulation range than conventional surface electrodes, providing distinct advantages in neural stimulation and recording [17]. Their design allows for precise control while minimizing impact on surrounding tissues. Moreover, when inserted deep within the body, they prove more effective than transcutaneous electrical stimulation. The minimally invasive nature of these electrodes—combined with immediate removal after treatment—enhances patient acceptability compared to implanted electrodes [18]. Thus, combining biomaterial technology with needle electrodes emerges as one of the most feasible and clinically significant strategies for enhancing electrical stimulation therapy.

To enhance needle electrodes via biomaterial technology, a primary focus must be on increasing drug loading capacity and delivery efficiency. While previous studies have documented the development and application of coated needles [19], challenges in drug delivery persist. These include limited drug loading capacity, vulnerability to skin barriers, and localized burst release. Our research team has previously introduced spiral microneedles [20], which feature a unique grooved structure that facilitates localized drug delivery. The advantages of these microneedles lie in their length, flexibility, and penetrative ability, enabling them to effectively target various deep-seated or resistant tissues for drug administration. Notably, the parameters of the grooves can accommodate different biomaterials, such as microspheres and liposomes, promoting local sustained drug release and enhancing therapeutic effects [21]. By incorporating targeted drugs into spiral microneedles, we have successfully delivered medication to tissues beneath the cartilage layer—an area challenging to reach with conventional local delivery methods—resulting in favorable treatment outcomes [15]. Furthermore, spiral microneedles offer a significant advantage as they not only serve as delivery tools but also act as platforms for the integration of multiple therapeutic approaches. This synergistic combination enhances efficacy by regulating relevant mechanisms. For instance, when combined with thermal therapy, drug-loaded spiral microneedles have shown potential in modulating mitochondrial function, thus revealing promising applications [20]. Not only do spiral microneedles share a similar diameter with traditional acupuncture needles, both being crafted from 304 stainless steel, but their conductive properties suggest they could function as electrodes [22]. However, the threaded microneedle electrodes need to be further improved, for example, to further reduce the irritation and discomfort of the threaded structure on the tissue [23], and to increase the likelihood of breakage or damage of the needles at the same diameter compared to the conventional acupuncture needles [24]. Dopamine combined with chitosan not only due to its exact adhesion effect [25] but also due to its good biocompatibility and beneficial effects on tissue regeneration [26, 27]. By applying a polydopamine and chitosan coating to improve adhesion, we have further enhanced the drug loading capacity and delivery efficiency through the incorporation of liposome microspheres embedded in the grooves of the spiral microneedles [28]. Therefore, advancing the spiral microneedle technology as an electrode system is highly feasible for achieving precise in-situ three-dimensional drug delivery to the core region during electrical stimulation, effectively mitigating issues related to electrical overload.

Peripheral nerve injury (PNI) is a common clinical challenge where bioelectric stimulation is frequently employed [29]. However, electrical stimulation is also difficult to achieve full recovery of nerve function after injury, and “electrical overload” can impede tissue and cellular recovery following injury, thereby affecting the restoration of nerve function [30,31]. To tackle this problem, our research team has developed a spiral microneedle electrode system designed for precise synchronous drug delivery to the core region affected by “electrical overload” during electrical stimulation. Vitamin B12 (VB12), recognized for its neuroprotective properties, and vitamin E (VE) succinate, which plays a role in combating oxidative stress [32], are key nutrients that can alleviate the cellular damage associated with electrical stimulation. Their localized application ensures both efficacy and biosafety. We have

utilized alkylated VB12 and VE succinate liposome microsphere complexes [33], which are released in a controlled manner within the core area of “electrical overload” facilitated by the spiral microneedle electrode. To enhance the loading efficiency of microspheres into the grooves of the spiral microneedle, we implemented electrostatic coating modifications alongside techniques such as freeze-drying and expansion scaling. Initially, a polydopamine coating was applied to the base of the spiral microneedle under alkaline conditions [34,35]. This was followed by the formation of a chitosan gel layer on the needle surface through covalent bonds, hydrogen bonding,  $\pi$ - $\pi$  stacking, and other interactions involving dopamine and various functional molecules. Subsequently, shrinkage microspheres prepared by freeze-drying were embedded into the needle groove via electrostatic adsorption. During electrical stimulation, the spiral microneedles functioned as electrode needles, wherein the microspheres absorbed moisture, expanded, and subsequently detached from the needle tip utilizing twisting operations, thus achieving in-situ targeted delivery [36]. *In vitro* experiments demonstrated that these microspheres effectively alleviated oxidative stress induced by electrical stimulation and provided protective effects for cells. *In vivo* studies confirmed that the spiral microneedles could successfully deliver the microspheres to the core region experiencing “electrical overload” while facilitating sustained drug release. This approach significantly enhanced the local tissue’s antioxidant capacity and improved the efficacy of electrical stimulation in treating PNI. In conclusion, our spiral microneedle electrode system allows for precise drug delivery to the core area during electrical stimulation, effectively inhibiting “electrical overload” while enhancing both the safety and therapeutic outcomes of electrical stimulation in PNI treatment (see Scheme 1).

## 2. Material and methods

All reagents used, unless otherwise specified, were obtained from Shanghai Aladdin Biochemical Technology Co., Ltd.

### 2.1. Preparation and characterization of drug-loaded liposomes

Alkylated VB12 was synthesized from unmodified VB12 using n-octadecylamine and 1,1'-carbonyldiimidazol (CDI) as the catalyst [37, 38]. In brief, 0.342 g of VB12 was dissolved in 10 mL DMSO, followed by the addition of 50 mg CDI and stirring for 20 min under nitrogen at room temperature. Next, 54 mg of n-octadecylamine and two drops of triethylamine (TEA) were added, and the mixture was stirred for an additional 24 h under similar conditions. The reaction was monitored by thin layer chromatography (TLC) with a solvent of dichloromethane/methanol/water (65/25/4). The mixture was diluted with 200 mL dichloromethane and washed three times with saturated salt solution. The organic phase was collected, and the solvent was evaporated to obtain the crude product, which was then purified by column chromatography using dichloromethane/methanol (5/1), yielding approximately 40 %.

Subsequently, drug-loaded liposomes were prepared using the thin-film dispersion method [39]. A lipid mixture of lecithin, cholesterol, alkylated VB12, and VE succinate was dissolved in dichloromethane (molar ratio 70:20:5:5) and evaporated to form a thin film. PBS was added for hydration for 30 min at 25 °C, followed by ultrasonication at 50 % power (325 W) with a frequency of 0.5 Hz for 10 min, interrupted twice for cooling.

Laser particle analysis measured the size and zeta potential of the liposomes (Malvern Ltd., UK). Morphological structure was observed using transmission electron microscopy (TEM) (FEI Co., USA) and scanning electron microscopy (SEM) (FEI Co., USA). Drug loading and encapsulation efficiency were assessed by the dialysis method with UV spectrophotometry (Thermo Co., USA) [40].



## 2.2. Preparation and characterization of HAMA microspheres

Firstly, HAMA was synthesized as previously reported [41]. Briefly, a mixture of 10 g of HA and 20 mL of methacrylic anhydride (MA) reacted overnight in an alkaline state with 5 M NaOH. After stirring for 8 h, the mixture underwent subsequent dialysis over 3 days and was then freeze-dried to obtain HAMA powder.

For the preparation of HAMA microspheres, a well-established microfluidic method was employed as previously described [41]. In brief, HAMA (3 wt%, including 0.5 wt% photoinitiator) was dissolved in PBS or a liposomal aqueous phase containing 1 mM each of VB12 and VE as the water phase. An oil phase consisting of a 5 wt% Span 80 paraffin oil solution was introduced into a microfluidic device (LongerPump Co., China). The flow rates of the water and oil phases were adjusted using a microinjection pump to produce microspheres approximately 200  $\mu\text{m}$  in diameter, ensuring uniformity. After that, crosslinking was performed under UV for 10 min to obtain HAMA hydrogel microspheres. After washing quickly with diethyl ether 3 times at room temperature, followed by washing slowly with dd H<sub>2</sub>O 3 times (1 h at a time) at 4 °C temperature, the HAMA microspheres were freeze-dried for use.

The primary configuration and dimensions of HAMA microspheres were examined using a bright-field microscope, while the coating arrangement and dimensions of freeze-dried microspheres were observed with SEM.

## 2.3. Physicochemical characterization of HAMA microspheres

Drug release from HAMA microspheres was assessed using UV spectroscopy [42,43]. In brief, 10 mg of HAMA microspheres was suspended in 5 mL of PBS (pH 7.4, 37 °C), and hyaluronidase was introduced at a concentration of 150 U/L for digestion. The enzyme solution was replenished every 2 days to maintain its activity [21]. HPLC (Agilent Co., USA) was utilized to measure drug concentrations in PBS solutions at various time intervals (0.5, 2, 4, 24, 48, 72, 168, 336 h) for determining drug release. Additionally, the degradation of microspheres was observed under a bright-field microscope at 7 and 14 days.

The swelling behavior was evaluated following a previous protocol [44]. In short, 3 mg of microspheres was placed in a 1.5 mL tube, weighed together with the tube, and then 1 mL of deionized water was added. The suspension's pH was adjusted to 7.4, and the tube was placed in a shaking incubator (Thermo Co., USA) at 37 °C and 80 rpm. At specified time points (0.5, 2, 4, 24, 48, 72 h), the tubes were centrifuged (3000 rpm, 3 min), the supernatant was discarded, excess water was blotted using filter paper, and the microspheres were reweighed until a constant weight was achieved.

## 2.4. Preparation and characterization of threaded microneedle-microsphere system

Previous research demonstrated the successful use of threaded microneedles in localizing lesions for treating osteoarthritic rats [15, 20]. The microneedles were created by adding threaded grooves with specific dimensions to stainless steel needles. These grooves could be customized for different experimental animals. The structure of the grooves was examined visually and under a microscope. The mechanical properties of the microneedles were evaluated by comparing them to medical acupuncture needles during needle-holding tests. Following fabrication, the microneedles were soaked in a dopamine solution overnight at room temperature. Coating was achieved through the self-polymerisation reaction of dopamine in a weak alkaline environment on the surface of the threaded microneedles. Subsequently, by allowing dopamine to form covalent bonds, hydrogen bonds,  $\pi$ - $\pi$  stacking, etc., with different functional molecules, the needles were immersed in a 5 % chitosan solution, forming a chitosan gel coating on the surface through intermolecular forces. We used a precision analytical balance Cubis® II (Sartorius, DE) to weigh 0.2 mg/needle of

freeze-dried microspheres and adhere them to the grooves of the needle body. Manual counting confirmed that the number of loaded microspheres was basically the same (Fig. S13). Finally, the freeze-dried microsphere powder was adhered to the needles through the physical viscosity and electrostatic adsorption of polydopamine chitosan co-deposited coatings. About 2 mg on each needle. The microspheres on the needles were embedded in the grooves through vacuum drying, the thread microneedle electrode was obtained. By introducing Cy5.5 fluorescent microspheres onto the needles, the microneedles were used to pierce on HAMA hydrogel for 20 min to simulate *in vivo* environments, and the local delivery effect was observed under a fluorescent microscope. We inserted the thread loaded with rhodamine into pork tissue with skin, pulled it out 20 min later, and left it at 4 °C for 24 h before fixed embedding. Cross-sectional sections were taken from different depth layers of tissue from shallow to deep, and red fluorescence was observed under a fluorescence microscope after DAPI staining of nuclei.

## 2.5. Biocompatibility assessment

RSC96 cells, a common cell line used in peripheral nerve research, were cultured in high-glucose DMEM supplemented with 10 % FBS. The cytotoxicity of liposomes and microspheres on the cells was assessed using CCK-8 and cell live/dead staining kits (Beyotime Co., China). After seeding the cells in a 96-well plate, they were exposed to electrical stimulation the next day for 20 min, followed by treatment with liposomes or microsphere extracts. For CCK-8 testing, the working solution was added to each well on the third day, and absorbance was measured at 450 nm after 1 h of incubation. Cell live/dead staining involved removing the culture medium on the third day, washing the cells with PBS, adding a staining solution, and then observing under a fluorescence microscope. Live cells emitted green fluorescence, while dead cells emitted red fluorescence. Statistical analysis was performed using ImageJ software.

## 2.6. Measurement of oxidative stress levels

Cellular oxidative stress levels were assessed using three methods: ROS, MDA, SOD (Beyotime Co., China) and DPPH detection (MesGen Co., China). For ROS detection, cells were treated and then incubated with a DCFH-DA ROS detection kit at 37 °C for 20 min. The fluorescence intensity was measured with an ELISA reader at specific excitation and emission wavelengths. After treatment, suitable cells were added with a DCFH-DA fluorescent probe, incubated at 37 °C for 1 h, and washed with PBS 2 times, and fluorescence signals were detected by fluorescence microscope at an excitation wavelength of 480 nm and emission wavelength of 525 nm. For DPPH detection, according to the number of cells (10000): the extraction liquid volume (mL) was 500:1, and the cells were broken by ice bath ultrasonic wave (power 200 W, ultrasonic 3 s, interval 10 s, repeat 30 times); The supernatant was obtained by centrifugation at 4 °C for 10 min at 10000 g, and the detection reagent was added to read and calculate at the wavelength of 515 nm. MDA detection involved extracting proteins from collected cells using RIPA lysis buffer, and analyzing the lysate with an MDA detection kit after heating. Protein concentration was determined with a BCA assay. SOD detection required cell lysis with a specific solution, followed by a 30 min incubation with working solutions. Absorbance readings were taken to calculate SOD enzyme activity units, which were then normalized to protein concentration.

## 2.7. Preparation of animal experimental model

All surgical and experimental procedures on rats were approved by the Animal Ethics Committee, Finock Biotechnology Co., LTD (AUP-20241227-01). Wistar rats weighing  $260 \pm 20$  g were utilized following a one-week acclimatization period. To establish the sciatic nerve crush



injury model, the rats were anesthetized with pentobarbital sodium. The surgical procedure involved preparing the right gluteal area, disinfecting it with alcohol, and exposing the sciatic nerve by dissecting the muscle. The nerve was clamped three times for 10 s each using the same hemostatic forceps at the midsection of the sciatic nerve, followed by a 10-s release. The sciatic nerve was freed, and the procedure was repeated 3 times. The skin was sutured with 3-0 sterile silk thread and then disinfected with iodine. The surgical incision was closely monitored for signs of detachment or infection and appropriate measures were taken.

## 2.8. Grouping and treatment of animal experiments

After the rats were modeled, they were divided into distinct groups: Control, Model, Electrical Stimulation (Ele), Electrical Stimulation + Blank Microspheres (Ele + MS), and Electrical Stimulation + Drug-Loaded Microspheres (Ele + Lipo@MS), each consisting of 6 rats. Anatomically, the sciatic nerve plexus was precisely located 0.5 cm below the midpoint of the femur and at the center of the popliteal fossa in the hind limb. The acupuncture depth is about 1 cm (threaded section fully inserted) to deliver to the sciatic nerve of the rat. Utilizing extended acupuncture needles at these positions, an electrical stimulator (with the anode upstream and the cathode downstream) was connected to induce muscle twitching in the rats at a frequency of 5 Hz using an intermittent waveform (KWD-808, YINGDI Co., China). Each 20 min session was administered every other day for a total of 4 weeks to mimic clinical electrical stimulation.

## 2.9. General observation and functional indices after sciatic nerve injury

General observations and functional assessments were conducted post-sciatic nerve injury. Affected rats displayed limping and dragging of the right hind limb, with paler skin, muscle atrophy, and curled toes compared to the healthy side. Severe cases exhibited foot ulcers and toe loss, with noticeable improvement post-treatment. Recovery was evaluated through functional indices, including the nerve conduction velocity (NCV) ratio (injured side/healthy side) and the wet weight ratio of the gastrocnemius muscle (injured side/healthy side). The NCV ratio was determined by positioning stimulating and receiving electrodes along the sciatic nerve, utilizing the RM6240E multi-channel physiological signal acquisition system (Chengdu Instrument Co., China). Muscle samples from the gastrocnemius (WWRG) were weighed post-dissection from specific femoral locations to assess muscle atrophy due to nerve damage. The evaluation of functional indices entailed gait analysis to ascertain the sciatic nerve function index (SFI). The rats' paws were dipped in blue ink, and they traversed a narrow paper box lined with white paper. The foot impressions from both the healthy (N) and impaired (E) sides were recorded on the box's base, where the distances between the central toe and heel (PL), the first and fifth toes (TW), and the second and fourth toes (IT) were precisely measured. The SFI was subsequently derived using the formula:  $SFI = 100 - [-38.3 (EPL - NPL) / NPL + 109.5 (ETW - NTW) / NTW + 13.3 (EIT - NIT) / NIT - 8.8]$ . A perfect score of 100 denoted unimpeded function, whereas a score of 0 signified total impairment.

## 2.10. Assessment of microstructural regeneration post sciatic nerve injury

To assess the microstructural regeneration following sciatic nerve injury, immunohistochemical staining was employed. The regeneration of nerve fibers was observed through dual staining utilizing neurofilament 200 (NF200) and myelin basic protein (MBP), respectively, to label axons and myelin sheaths. Additionally, S100, a proliferation marker for Schwann cells, was used to detect the proliferation of these cells, thereby reflecting nerve regeneration. Furthermore, the expression levels of NGF, BDNF, and GDNF were evaluated due to their significant roles in the indirect responses pertaining to neuron survival, axonal

regeneration, and Schwann cell proliferation. The rats were anesthetized, and blood was collected from the abdominal aorta. Following this, the rats were euthanized to facilitate the immediate collection of sciatic nerve samples. The nerve samples were subsequently washed with PBS, fixed overnight in 4 % paraformaldehyde, and processed for paraffin sectioning. The subsequent steps included antigen retrieval, incubation with the respective antibodies, and fluorescence microscopy imaging (Olympus Co., Japan).

## 2.11. Detection of total antioxidant capacity of nerve tissue

Preparation of sciatic nerve tissue homogenates was focused on the core region, where needle and electrical stimulation were administered. Adhering to the kit's guidelines, the homogenates were sequentially combined with peroxidase and ABTS working solutions (Beyotime Co., China). Following 6 min of incubation at room temperature, the mixture enzyme activity was quantified at a 414 nm wavelength. Protein concentration was determined using the BCA method, and the total antioxidant capacity was subsequently calculated by normalizing the antioxidant capacity to the protein concentration.

## 2.12. Analysis of apoptotic cells via TUNEL assay

Apoptotic cell detection was performed using a one-step TUNEL detection kit (Beyotime Co., China). After deparaffinization and proteinase K treatment of paraffin-embedded sections at 37 °C for 20 min, a TUNEL detection solution was prepared and applied to the sections. The sections were incubated at 37 °C in a light-shielded environment for 1 h. Following this, cell nuclei were stained with DAPI, and fluorescence was observed under a fluorescence microscope (Olympus, Japan) at excitation and emission wavelengths of 550 nm and 570 nm, respectively.

## 2.13. In vivo imaging evaluation

For *in vivo* imaging, cy5.5-labeled liposomes were used to fluorescently label microspheres. These fluorescent microspheres were inserted into the sciatic nerve of rats using threaded long microneedles. Fluorescence intensity measurements at a 754 nm wavelength were recorded using the IVIS spectrum system (Xenogen, Hopkinton, MA) at various time intervals: 3 h, 24 h, 48 h, and 12 days. The observed fluorescence decay at these time points served as an indicator of the microspheres' slow drug release and *in vivo* degradation.

## 2.14. Proteomic detection

The total protein in the sample was extracted, part of the sample was taken out for protein concentration determination and SDS-PAGE detection, the other part was taken for trypsin enzymolysis and labeling, and then an equal amount of each labeled sample was mixed for chromatographic separation, and finally, the sample was analyzed by LC-MS/MS and data analysis.

## 2.15. Statistical analysis

All data were expressed as mean  $\pm$  SD. Statistical analyses were conducted using Student's t-test for pairwise comparisons and one-way analysis of variance (ANOVA) for multiple comparisons, with appropriate statistical software.

# 3. Results and discussion

## 3.1. Preparation and characterization of drug-loaded liposomes

For the threaded microneedle electrode system to efficiently encapsulate drugs, stabilize the sustained release, and improve the microenvironment after the *in-situ* stereotactic delivery of microspheres, we

utilized liposomes as the basic drug delivery tool, adopting the strategy of loading drugs into liposomes and encapsulating liposomes into microspheres [45]. Liposomes are small particles composed of phospholipids, cholesterol, and other components. Typically used in drug delivery systems, liposomes provide stable encapsulation for various drugs, ensuring protection and sustained release.

Liposomes were formulated employing the thin-film technique, followed by multiple rounds of sonication for homogenization. Two drugs were loaded into liposomes, including VB12 and VE succinate (Fig. 1A). VB12 is a classic neurotrophic drug known for its neuroprotective effects [46]. But water soluble VB12 always shows burst release from liposomal structures [47]. Therefore, we synthesized lipophilic VB12 derivative (alkylated VB12) with alkyl chain conjugation via a cleavable -NHCOO- structure, providing the lipotropic action with liposomal phospholipid tails for stable loading. Through the usual hydrolysis reaction, VB12 could be transferred once it is released. Details of  $^1\text{H}$  NMR spectra of VB12 and alkylated VB12 can be found in Figs. S1 and S2. In addition, the released VB12 could be found in the incubated mixture of alkylated VB12 aqueous solution (Fig. S3). Meanwhile, VE succinate is a well-known liposoluble antioxidant that helps eliminate ROS in tissue cells, combats oxidative stress, enhances mitochondrial function, and prevents cellular aging [48]. Two liposoluble compounds could be encapsulated into the hydrophobic domain of lipid bilayers efficiently, for delivering to the core region of the electrode for continuous cellular protection. In the figure, we have standardized the annotation of VB12, using “U-VB12” for chemically unmodified VB12 and “VB12” for alkylated VB12. In addition, the naming is simplified to “VEB” for both VB12 and VE when applied together. When liposome loading is used, the suffix “-L” is used, and the unloaded liposome is named “E-L”. When microsphere loading is used, the suffix “@MS” is used.

After loading VE succinate and alkylated VB12 into the liposome membrane structure, the particle size of the liposomes was determined to be approximately 91.3 nm, with a zeta potential of around  $-12.6$  mV (Fig. 1B and C). TEM and SEM revealed the typical phospholipid bilayer membrane structure and elliptical appearance of the liposomes (Fig. 1D, Fig. S4). At a wavelength of 361 nm, UV spectrophotometry revealed that the alkylated VB12 derivative displayed superior sustained release characteristics in comparison to the VB12 compound released from liposomes (Fig. 1E). Liposomes showed good stability within 30 d (Fig. S5), and liposomes loaded with alkylated VB12 showed no significant difference on cell viability compared with unmodified VB12 at 24 and 48 h (Fig. S6).

### 3.2. Preparation and characterization of the threaded microneedle electrode system

Using microfluidic technology, various functional microspheres can be prepared [49]. In our previous studies, utilizing photo-crosslinkable hyaluronic acid methacrylate (HAMA), synthesized via the esterification reaction between hyaluronic acid (HA) and methacrylic anhydride (MA) under alkaline conditions, mature porous hydrogel microspheres were successfully fabricated [50,51]. Subsequently, dialysis was performed to remove impurities, followed by freeze-drying (Fig. 1F). Subsequently, microfluidic technology was employed to fabricate uniform hydrogel microspheres [52,53], and UV crosslinking was carried out through rapid oil-phase cutting and slow water-phase processing [54]. Liposomes were suspended in the aqueous phase during the microfluidic process. The structure of hydrogel microspheres enables sustained and targeted drug release, consequently, therapeutic efficacy is enhanced, while undesirable side effects are mitigated [55], while possessing good biocompatibility [56]. They can be customized according to specific drugs, treatment sites, and requirements to improve treatment specificity and effectiveness [57]. Composite carriers composed of microspheres and liposomes achieve sustained release [21]. Bright-field microscopy analysis depicts the microspheres with an approximate particle size of  $200\text{ }\mu\text{m}$ , as exhibited in Fig. 1G. Following freeze-drying,

the microspheres were further inspected under scanning electron microscopy, displaying an optimal circular morphology adorned with a porous surface structure (Fig. 1J). Compared to traditional hydrogels, porous structured microspheres increase surface area, enhancing drug protection and delivery capabilities [58]. Microfluidic microspheres have advantages such as monodispersity, uniform size, and versatility [59]. Moreover, they promote sustainable local delivery of drugs, even for nanoscale carriers like liposomes [60], and have the potential for repairing nerve injuries [61]. The *in vitro* degradation process of microspheres lasted approximately 14 days (Fig. S7). Compared to blank microspheres, liposome-loaded microspheres showed lower swelling characteristics (Fig. 1I). Furthermore, the microspheres exhibited stable sustained drug release for up to 14 days (Fig. 1H), thereby aiding in continuously improving the local microenvironment. In addition, according to the drug concentration in the solution, we calculated that the microspheres initially loaded VB12  $0.823\text{ }\mu\text{mol/g}$  and VE  $0.889\text{ }\mu\text{mol/g}$ . At 48 h and 72 h, the corresponding drug concentrations ( $\mu\text{M}$ ) of microsphere extracts were 0.497 (VB12) and 0.9117 (VE) at 48 h and 0.827 (VB12), 0.972 (VE) at 72 h. The drug release of the microspheres at 48/72 h meets the concentration required for good cellular compatibility (within  $1\text{ }\mu\text{M}$ ) (Fig. S8).

Needle electrodes are commonly used electrodes in electrical stimulation therapy for PNI [62]. Drawing inspiration from traditional Chinese acupuncture needles, we fabricated a threaded long micro-needle (Fig. 2A and B). It possesses a similar diameter, flexibility, as well as penetration, and flexibility to medical acupuncture needles (Fig. S9). The needle was coated with polydopamine by immersing it in a dopamine solution. However, simple dopamine adsorption is weak. Subsequently, it was immersed in a chitosan solution to prepare a polydopamine-chitosan co-deposition coating. The coating provided the needle with good adhesion through electrostatic attraction and physical stickiness. Then, the freeze-dried microspheres were attached to the needle and embedded into the grooves through vacuum drying (Fig. 2C). This scheme combines the self-polymerisation properties of dopamine with a coating construction strategy for the biocompatibility and antimicrobial properties of chitosan. On the one hand, the coating formed by dopamine self-polymerisation can enhance the adhesion of polymers such as chitosan [63]. Especially on the surface of some hydrophobic materials (e.g., metals, plastics, etc.), the dopamine film can provide a good adhesion basis for the subsequent chitosan coating; on the other hand, the dopamine film can not only provide physical adhesion, but also further optimize the performance of the coating through covalent binding or electrostatic interactions of its amine and phenolic hydroxyl groups with molecules such as chitosan [64]. In conclusion, this strategy enables the fabrication of a high-performance coating that provides both good adhesion and biocompatibility, antimicrobial and other properties. Long microneedles loaded with fluorescent microspheres were observed under a microscope to successfully deliver microspheres *in-situ* after an insertion and removal process in a hydrogel (Fig. 2D). Further, we inserted thread microacupuncture loaded with red fluorescence into pork tissue with skin, and found that red fluorescence existed in tissues of different depth levels, indicating that threaded microneedle electroacupuncture had better ability to achieve 3D stereoscopic delivery through human tissue barrier (Fig. 2E).

### 3.3. Biocompatibility and antioxidative stress evaluation of protective liposomes

Schwann cells constitute the primary neuroglial components within the peripheral nervous system, they form myelin sheaths around axons in peripheral nerves and are the primary cells in the area of injury. Schwann cells not only protect axons, but also have close material and signal exchange with neurons and play important roles in regeneration after nerve injury. After peripheral nerve injury, axon breakage and disintegration occur, and Schwann cells and macrophages are responsible for phagocytosis of disintegrated axon fragments [65], migrating

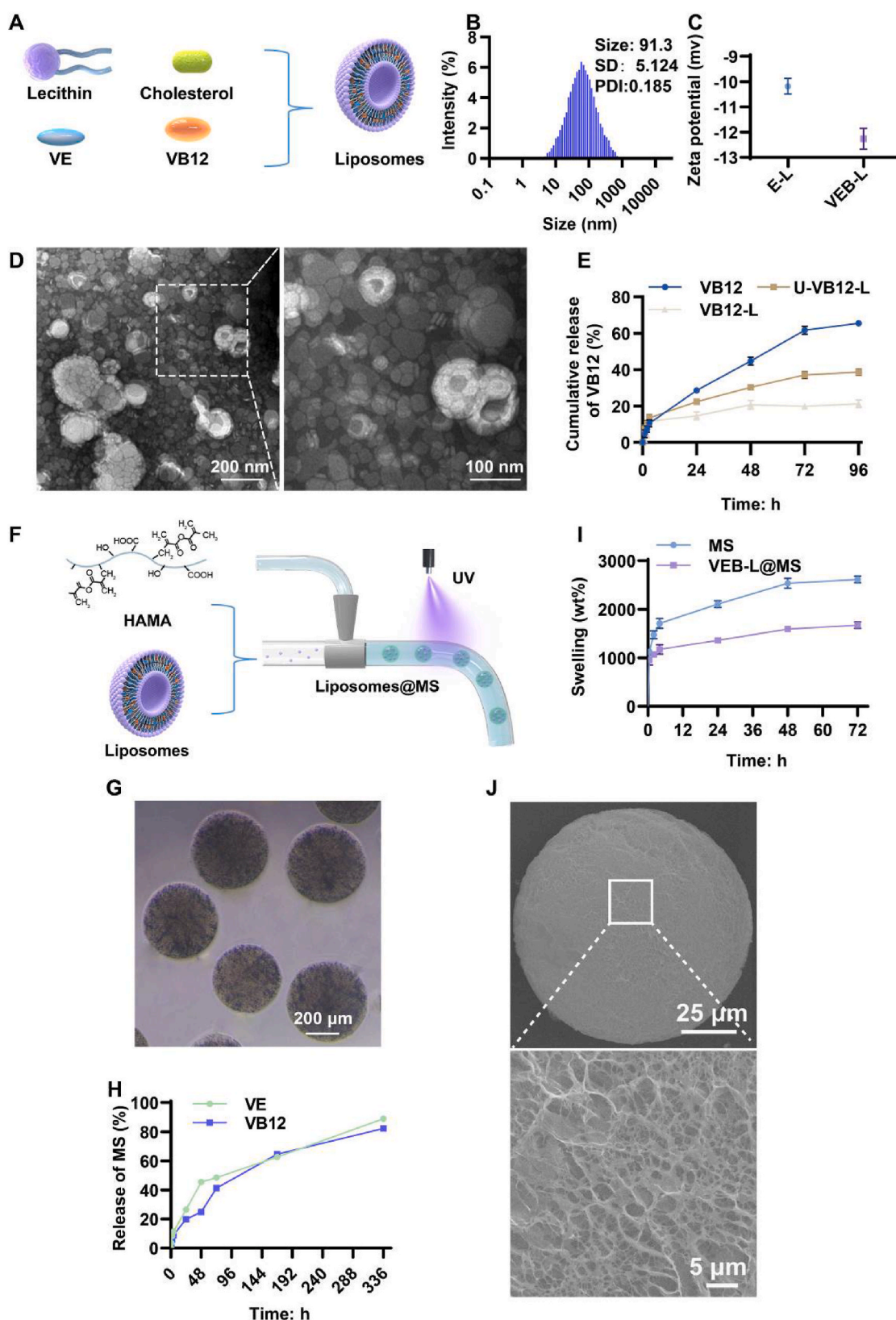


**Fig. 1.** Fabrication and characterization of liposomes and HAMA microspheres. (A) Liposomes loaded with VB12 and VE succinate. (B, C) DLS analysis of liposome size and zeta potential. (D) TEM observation of liposome structure. (E) UV spectrum analysis of liposomes for sustained release of VB12, U-VB12-L, VB12-L through dialysis. (F) Synthesis of HAMA microspheres using drug-loaded liposomes. (G) Bright-field microscopy observation of microspheres. (H) UV spectrum analysis of microspheres for the sustained release of VB12 and VE succinate. (I) Measurement of the swelling properties of microspheres. (J) Scanning electron microscopy observation of microspheres.



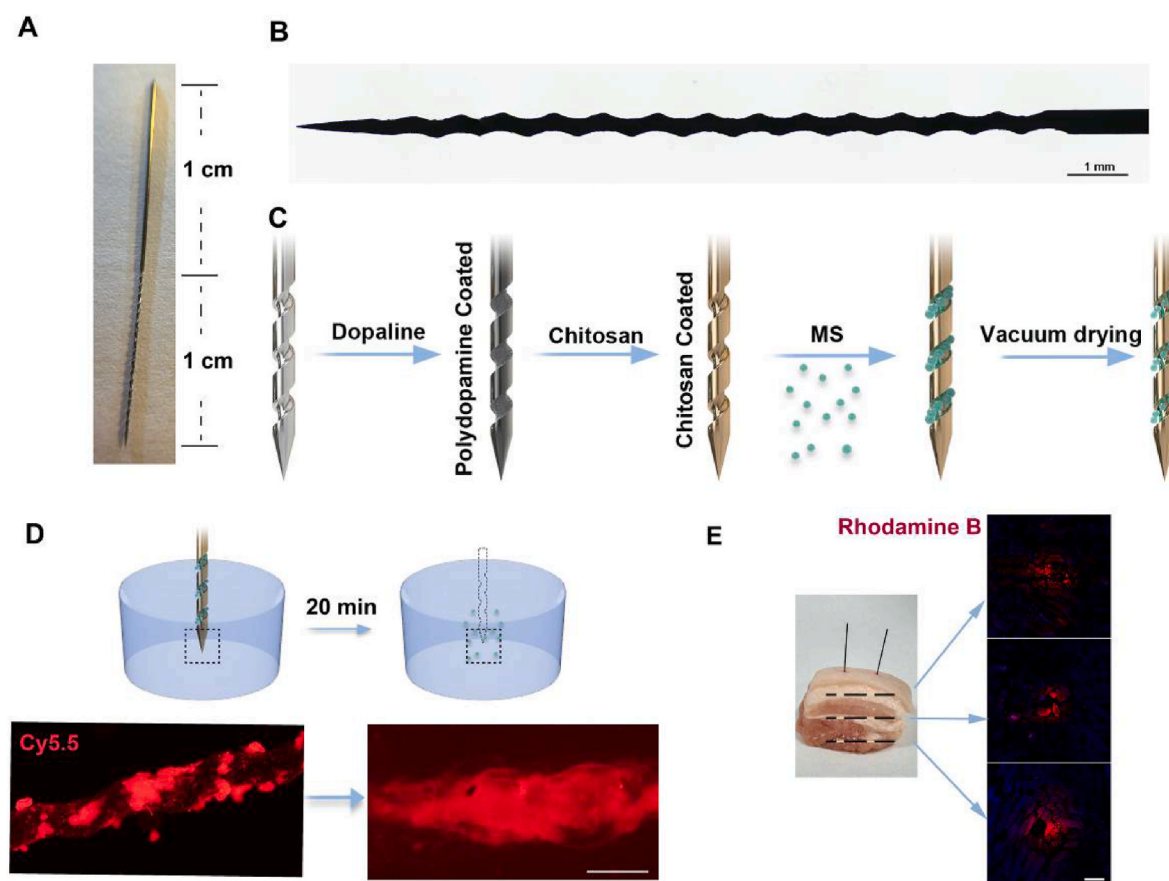


**Fig. 2.** The preparation and characterization of threaded microneedle electrode system. (A) Overall view of the long microneedle. (B) Structural observation of the threaded long microneedle under bright-field microscopy. (C) Using polydopamine and chitosan coatings, the embedding of threaded microneedle electrode system. (D) The threaded microneedle electrode system was observed under a fluorescence microscope to deliver red fluorescent microspheres *in-situ* in the hydrogel (Bar = 250  $\mu$ m). (E) The threaded microneedle electrode system was observed under a fluorescence microscope to deliver red fluorescent microspheres *in-situ* in the fresh pork with skin on (Bar = 200  $\mu$ m).

and directing neuronal axon neogenesis [66], and secreting a variety of neurotrophic factors to improve the nerve regeneration microenvironment and help damaged neurons to survive [67], and regulating neurons by delivering miRNA through exosomes [68–70]. Literature reports show that the Schwann cell line does not differ much from primary Schwann cells and can be a good substitute for primary cells [71,72], thus we utilized the rat Schwann cell line (RSC96) for cellular experiments [73]. Initially, cell viability assays were conducted to determine appropriate drug concentrations at the liposome level, with each drug screened individually. The CCK-8 assay was utilized to evaluate cell viability, revealing that liposomes loaded with concentrations below 10  $\mu$ M of VE succinate and 25  $\mu$ M of VB12 had no negative impact on cell viability, and even exhibited some enhancing effects (Fig. 3A and B). Subsequently, we evaluated the combined effects of the two drugs at different ratios on cell viability, finding that the ratio of 1:1 and a working concentration below 5  $\mu$ M were most suitable (Fig. 3C).

Despite the rapid development of piezoelectric biomaterials in neural tissue engineering, the bioelectric stimulator is still the mainstream due to its controllability, adaptability, and high efficiency [74]. Since the basic mechanism of electrical stimulation is to act between the tissues of the body through two electrodes of positive and negative poles, coupled with different tissues, distance length, etc. will lead to different regions of cells affected by electrical stimulation to different degrees. Oxidative stress is currently an important mechanism by which electrolytic products and excessive current affect cells [75–77]. The oxygen atom is one of the primary effects of high electric field potential on cells [78]. Exposure of cells to high electric field potential may disrupt the balance

of redox reactions. Additionally, the increased production of electrolysis byproducts within the core region of the electrode under high electric field potential can also induce oxidative stress. These ROS and electrolysis byproducts may induce oxidative stress, this damage encompasses vital cellular biomolecules, including proteins, lipids, and DNA, and triggers a cascade of cell signaling pathways, potentially culminating in adverse outcomes such as cell apoptosis or inflammatory reactions, thereby significantly impacting cellular function and survival [79,80]. Therefore, we evaluated the impact of protective liposomes on electrically stimulated cells through antioxidant stress assessment. The induction of oxidative stress by electrical stimulation has been reported [76] and is positively correlated with the intensity of the electric field [81]. By applying electrical stimulation to the cells, we observed that the generation of ROS increased gradually with the increase in current intensity (Fig. 3D and E). The current intensity of 2 mA can induce the increase of reactive oxygen species in cells, and there is a statistical difference. The cells themselves had the ability of self-regulation, and there was no statistical difference in cell viability at 24 h between 2 mA and 4 mA. However, when the current intensity continues to increase to 6 mA or above, great damage will be caused to cells at 24 h, indicating that cells can no longer resist excessive electrical stimulation through self-regulation. Based on the above considerations, we choose 4 mA below 6 mA as the fixed intensity for subsequent experiments (Fig. 3F).

The difference in the effects that can be produced by different electrical stimulation frequencies can be significant, therefore, we initially explored the effects of different frequencies on the cells. Cells were treated using three different frequencies, 1/5/100 Hz, with 4 mA

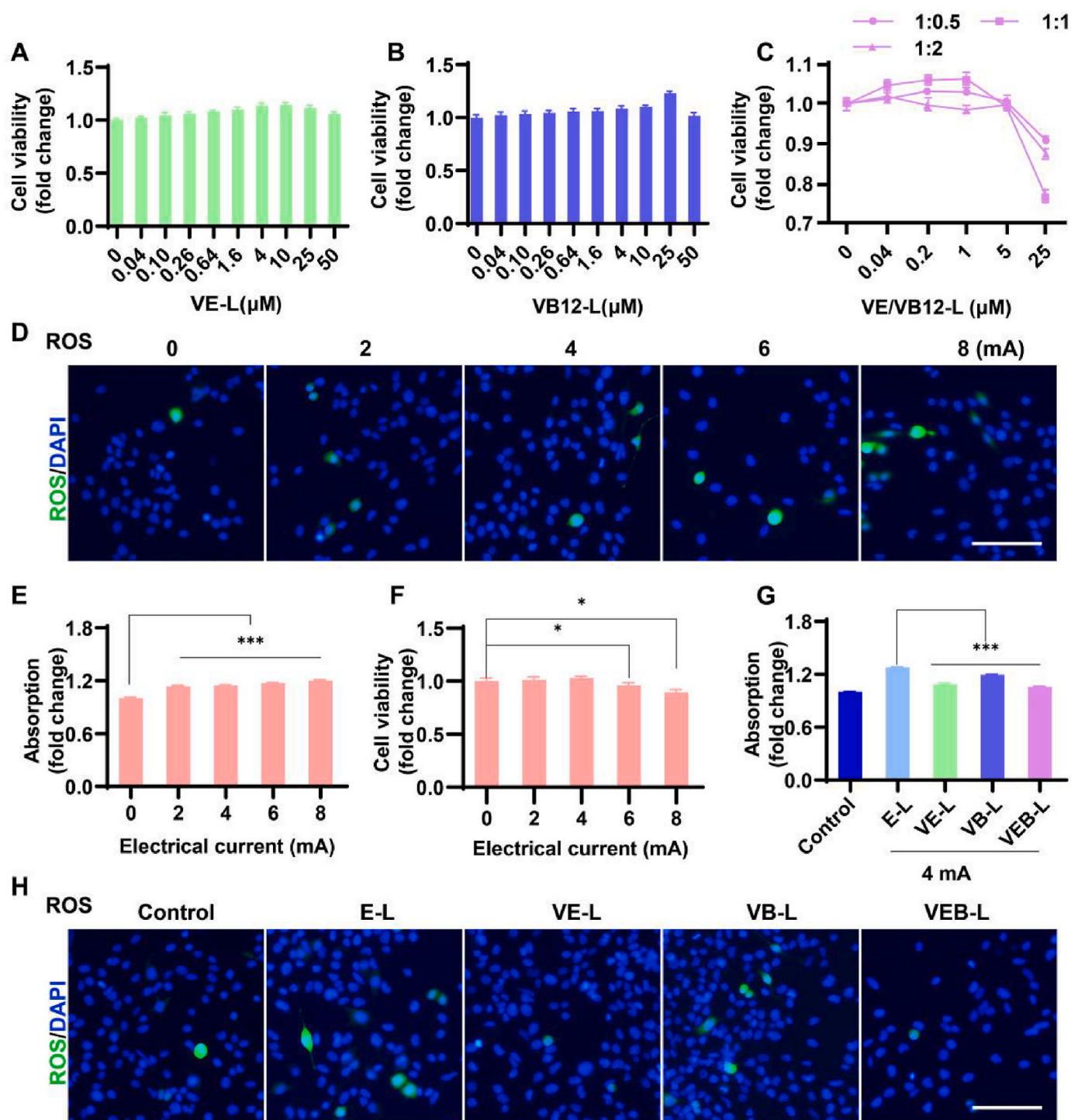


**Fig. 3.** The biological evaluation of liposomes. (A) CCK-8 assay to evaluate the impact of VE succinate liposomes on cell viability. (B) CCK-8 assay to evaluate the impact of VB12 liposomes on cell viability. (C) CCK-8 assay to evaluate the impact of VB12/VE succinate liposomes on cell viability. (D, E) Influence of current intensity on intracellular ROS expression. (F) Impact of current intensity on cell viability. (G, H) Influence of liposomes loaded with VE succinate, VB12, or VB12/VE succinate on ROS induction in electrically stimulated cells. (\* $P < 0.05$ , \*\*\* $P < 0.001$ , Bar = 100  $\mu\text{m}$ ).

current, and cell viability and ROS were examined. It was found that there was no significant change in cell viability at 1 Hz and 5 Hz, and when the frequency was 100 Hz, there was a slight decrease in cell viability. It shows that the frequency variation in smaller range has a weak effect on the cells, much less significant than the current intensity, which is consistent with the literature report [82], and the results of ROS have the same trend, suggesting that low-frequency electrical stimulation is less damaging to the cells (Fig. S11).

Compared to using VB12 alone (6.5 %), liposomes loaded with VE succinate could significantly reduce ROS levels (14.8 %) and increase DPPH free radical scavenging rate. The effect was even better when both drugs were loaded simultaneously (17.2 %) (Fig. 3G and H; Fig. S10), at the same time better reduced the current-induced cell death (Fig. 4A and B). The optimal effect was observed when both drugs were loaded at a 1:1 ratio with a concentration of 1  $\mu\text{M}$  by live-dead cell staining and cell counting (19.4 %) (Fig. 4C–E), and ROS staining further confirmed the

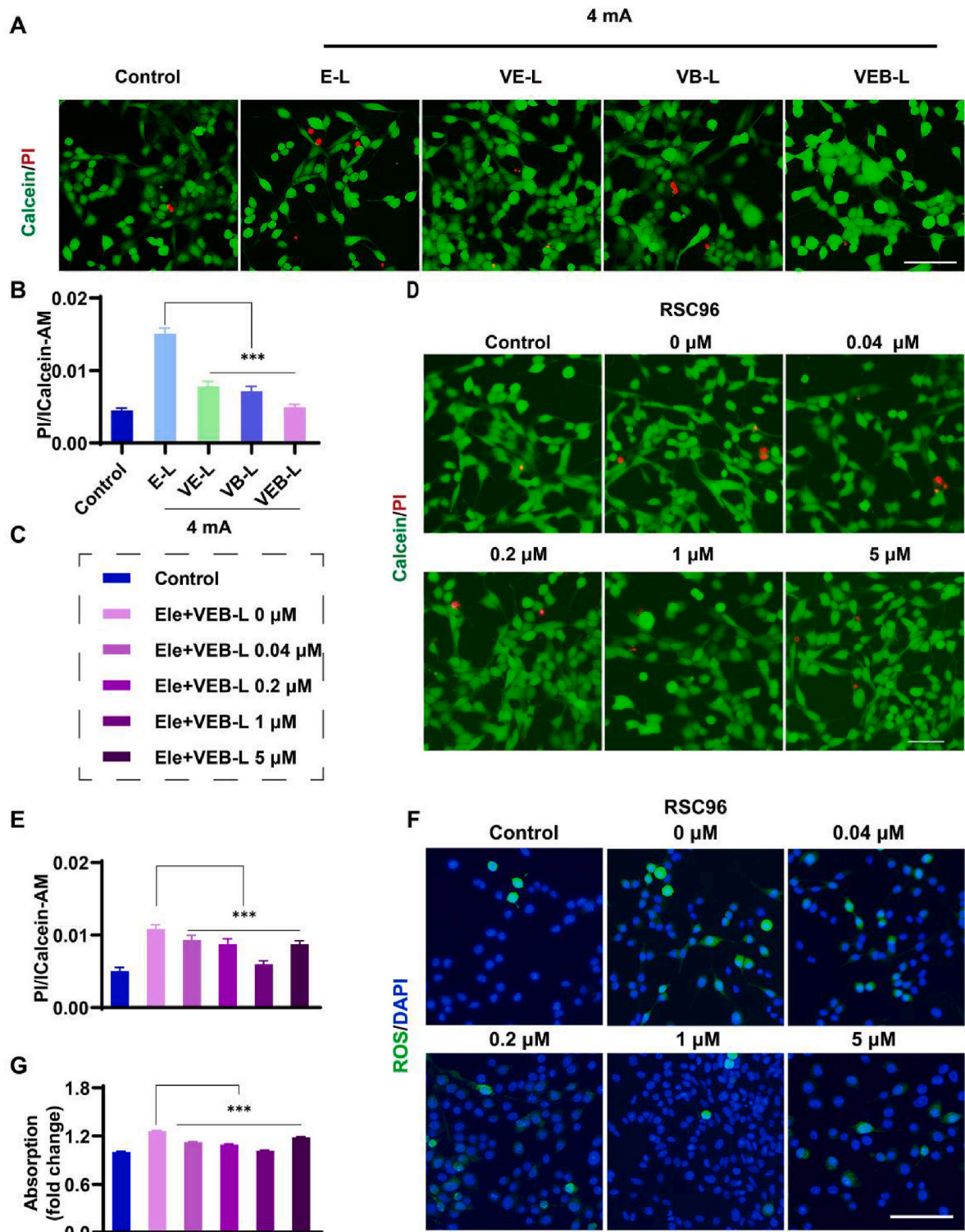


**Fig. 4.** The biological evaluation of liposomes. (A, B) Live/dead cell staining to evaluate the impact and statistics of liposomes on cell death induced by electrical stimulation. (C) Group introduction. (D, E) Live/dead cell staining to assess the effect and statistical data of liposomes loaded with different concentrations of VB12/VE succinate on cell death induced by electrical stimulation. (F, G) Impact of liposomes loaded with different concentrations of VB12/VE succinate on ROS induction in electrically stimulated cells. (\* $P < 0.05$ , \*\*\* $P < 0.001$ , Bar = 100  $\mu$ m).

protective effect of liposomes on electrically stimulated cells (Fig. 4F and G).

3.4. Biocompatibility and antioxidant stress evaluation of protective microspheres

Upon microscopic examination, we did not detect any statistically noteworthy variations in the cell viability of liposome-loaded microspheres (Lipo@MS) across the 1, 2, and 3-day intervals as revealed by



live/dead cell staining, which was further confirmed by CCK-8 assay (Fig. 5A–C). Cell death induced by electrical stimulation was alleviated by the protective microspheres (reduction by 59.5 %), indicating that microspheres loaded with VB12 and VE succinate liposomes could effectively mitigate the oxidative stress induced by electrical stimulation and protect the cells (Fig. 5D and E). Conductive hydrogels have the potential to synergistically enhance the efficacy of electrical stimulation, which inspires electrical stimulation combined with hydrogel microspheres [83]. Additionally, we measured key indicators of cellular oxidative stress: ROS, malondialdehyde (MDA), and superoxide dismutase (SOD) (Fig. 5F–I). Excessive ROS leads to lipid peroxidation, generating MDA. Accumulation of MDA serves as an indicator of the extent of oxidative stress, reflecting the degree of lipid oxidative damage [84]. SOD is an antioxidant enzyme mainly responsible for scavenging superoxide anions, serving as one of the key enzymes for cellular defense against oxidative stress. In an oxidative stress environment, the cell's self-protection mechanism leads to an increase in SOD activity to counteract the excessive accumulation of superoxide anions. Therefore, MDA is positively correlated with the level of oxidative stress, while SOD is negatively correlated [85]. The results indicated that the protective microspheres were able to reduce ROS induced by electrical stimulation (72.8 %). Electrical stimulation led to an increase in MDA and a decrease in SOD within the cells, while the application of protective microspheres decreased the induction of MDA (69.1 %) and increased SOD levels (81.2 %). In conclusion, our study demonstrates that liposomes and microspheres loaded with VB12/VE succinate exhibit good biocompatibility and can reduce cellular damage caused by electrical stimulation.

Neural differentiation is important for nerve regeneration, and we treated bone marrow MSCs using electrical stimulation and microsphere system to detect fluorescent expression of  $\beta$ III-Tubulin, capturing the presence of positivity, validating the inducing effect of electrical stimulation on the stem cells towards neural differentiation, and preliminarily confirming that the combined microsphere system can further promote nerve regeneration (Fig. S12).

### 3.5. Evaluation of the therapeutic effect of threaded microneedle electrode system on nerve injury

The ultimate goal of our research is for the threaded microneedle electrode system to alleviate local “electrical overload”, thereby enhancing the therapeutic effects of electrical stimulation. After successfully confirming the protective effect of microspheres on cellular “electrical overload” *in vitro*, we evaluated the *in vivo* application of the threaded microneedle electrode system through assessments of nerve injury treatment effects. We employed a sciatic nerve injury model in rats, inducing compression injury to the right sciatic nerve. Post-injury, rats exhibited dragging of the right hind limb and curling of the toes, with severe cases possibly developing skin ulcers and toe necrosis.

Following modeling, we administered electrical stimulation therapy using long microneedle electrodes while concurrently delivering microspheres *in-situ* (Fig. 6A). The main advantages of using threaded microneedle electrodes to deliver microspheres are as follows: 1. wider delivery range: for example, the microspheres can be delivered to the subchondral layer, which is not possible with syringes; 2. smaller damage: due to the smaller diameter and solid structure than syringes, the damage to the tissue is smaller and the pain caused is also smaller; 3. more precise targeting: the substantial metal structure is flexible, and it can be adjusted to the direction of the needle after insertion, just like needles. More precise targeting: the metal structure of the substance is flexible and can be adjusted to the direction after needle insertion as well as needle puncture; 4. More potential for combining with a variety of physical therapy methods: after the puncture, it can be connected to a variety of physical therapy equipment such as electrical stimulation, thermal stimulation, etc. Combined with the microspheres delivered by needles, it can be targeted to minimize the possible damage of physical therapy and amplify the therapeutic effect [15,20,22].

Long microneedles were inserted along the damaged sciatic nerve as the needle electrodes (Fig. S14). Subsequently, electrical stimulation was applied using an electroacupuncture device, the microspheres loaded on the needle absorbed bodily fluids and swelled, while the chitosan medium undergoes shear-thinning upon twisting manipulation. Because the grooves of the needle body are continuous spirals starting from the tip, it is possible to release the microspheres uniformly at different levels to ensure their distribution, prompting the microspheres to detach *in-situ* under twisting manipulation, thereby achieving *in-situ* stereotactic delivery. This method aims to use the microneedle electrode to deliver drugs *in situ* to counter “electrical overload” in the core area of the electrode, to reduce the unnecessary damage caused by an uneven distribution of the electric field, and to improve the curative effect of electrical stimulation. After 4 weeks, assessments were conducted on gross observation of the toes (Fig. S15), nerve conduction velocity, gastrocnemius muscle wet weight ratio, and footprint analysis, among other functional recovery indicators. Nerve conduction velocity measures the speed at which nerve impulses propagate along the nerve conduction pathway, serving as an evaluation of whether nerve conduction is disrupted or damaged. Nerves play a role in governing and nourishing muscles, and muscle atrophy following nerve injury leads to weight loss, reflecting the severity of nerve damage and recovery. Footprint analysis is a widely used non-invasive method in experiments to reflect sciatic nerve function [86]. The results indicated a loss of sciatic nerve function in the model rats (Fig. 6B–E) [87]. Electrical stimulation therapy improved nerve function, with the combination of drug-loaded microspheres further promoting functional recovery compared to using electrical stimulation alone or blank microspheres with electrical stimulation. Long microneedle electrodes showed improvements in nerve conduction velocity ratio (41.9 %), gastrocnemius muscle wet weight ratio (4.3 %), and sciatic nerve function index (12.1 %) compared to sole electrical stimulation.

The sciatic nerve is composed of myelinated nerve fibers, including axons and surrounding myelin sheath. Normal nerve fibers exhibit a regular and orderly concentric structure. Structural breakdown following nerve injury can be evaluated based on the integrity of the structure, Wallerian degeneration occurs after peripheral nerve injury, where the axonal and myelin structures undergo major destruction and then neogenesis after injury [88], reflecting the extent of nerve damage and recovery. Immunofluorescence staining revealed significant disruption in the axon and myelin sheath structures within the nerve microstructure post-modeling (Fig. 6F–H) [89]. Histological structures of the nerve injury areas in each group were observed through HE staining (Fig. 6I), where the Control group exhibited numerous regular concentric structures (indicated by arrows, with circles representing myelin sheath and blue-brown dots at the center indicating axons). After modeling, extensive structural damage and reduced axon quantity ( $17.4 \pm 7$ ) were observed, with electrical stimulation therapy increasing the number of axons ( $44.7 \pm 4.9$ ). The combination of electrical stimulation and long microneedle treatment led to more extensive reshaping of concentric structures ( $85.4 \pm 5$ ), indicating that delivering microspheres *in-situ* through long microneedle electrodes contributes to enhancing the efficacy of electrical stimulation.

Immunoreactivity between the microneedle and tissue interface is an interesting topic due to the rigid material characteristics of microneedles, and foreign body reactions caused by mechanical mismatches at the tissue interface. Traditional needling, as well as electroacupuncture, can have an impact on immunity. Immunomodulation of the local microenvironment due to the microtraumatic environment generated by needling includes induction of a local sterile inflammatory response (recruitment of macrophages and neutrophils) [90], deformation of connective tissues and effects on stretch-sensitive cells (activation of fibroblasts and macrophages) [91], through crosstalk between the nervous system and the immune system (different nerve fibers acted upon, sensations produced, and responses elicited by needling different sites and tissues, as well as projections to brain regions, and mediate the

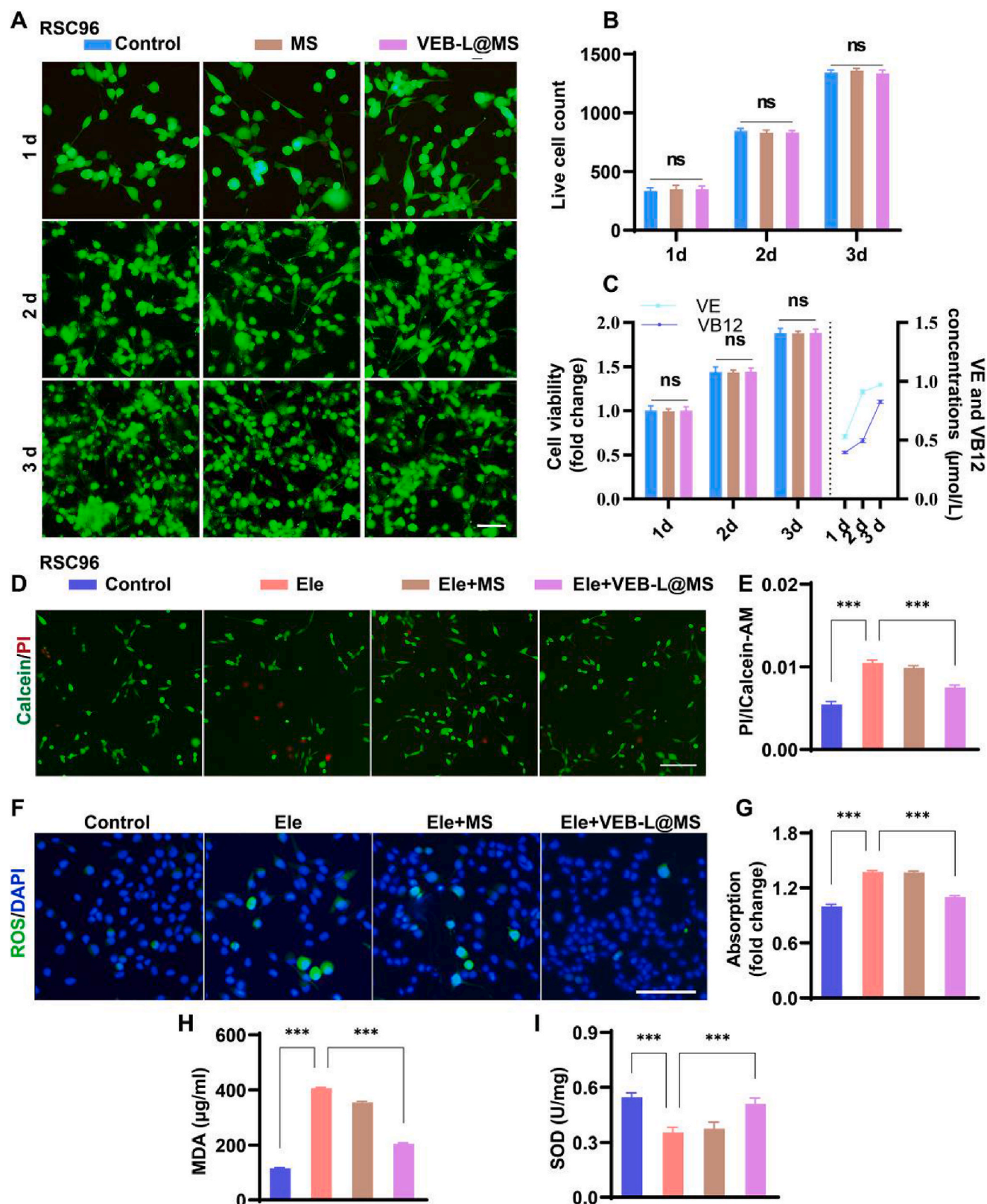


**Fig. 5.** The cell toxicity of microspheres and their ability to inhibit “electrical overload”. (A, B) Live/dead cell staining to assess the impact and statistics of blank microspheres and drug-loaded microspheres (Lipo@MS) on cell viability within 3 days (Bar = 50  $\mu$ m). (C) CCK-8 assay to evaluate the effect of blank microspheres and drug-loaded microspheres on cell viability within 3 days, the right y-axis and curves reflect the microsphere slow-release VE and VB12 data. (D, E). Influence of blank MS and Lipo@MS on cell survival rate induced by electrical stimulation, live/dead cell staining, and counting (Bar = 200  $\mu$ m). (F, G) Impact of blank MS and Lipo@MS on ROS induction in electrically stimulated cells (Bar = 100  $\mu$ m). (H, I) Effect of blank MS and Lipo@MS on MDA and SOD generation in electrically stimulated cells (\*\*\* $P < 0.001$ ).



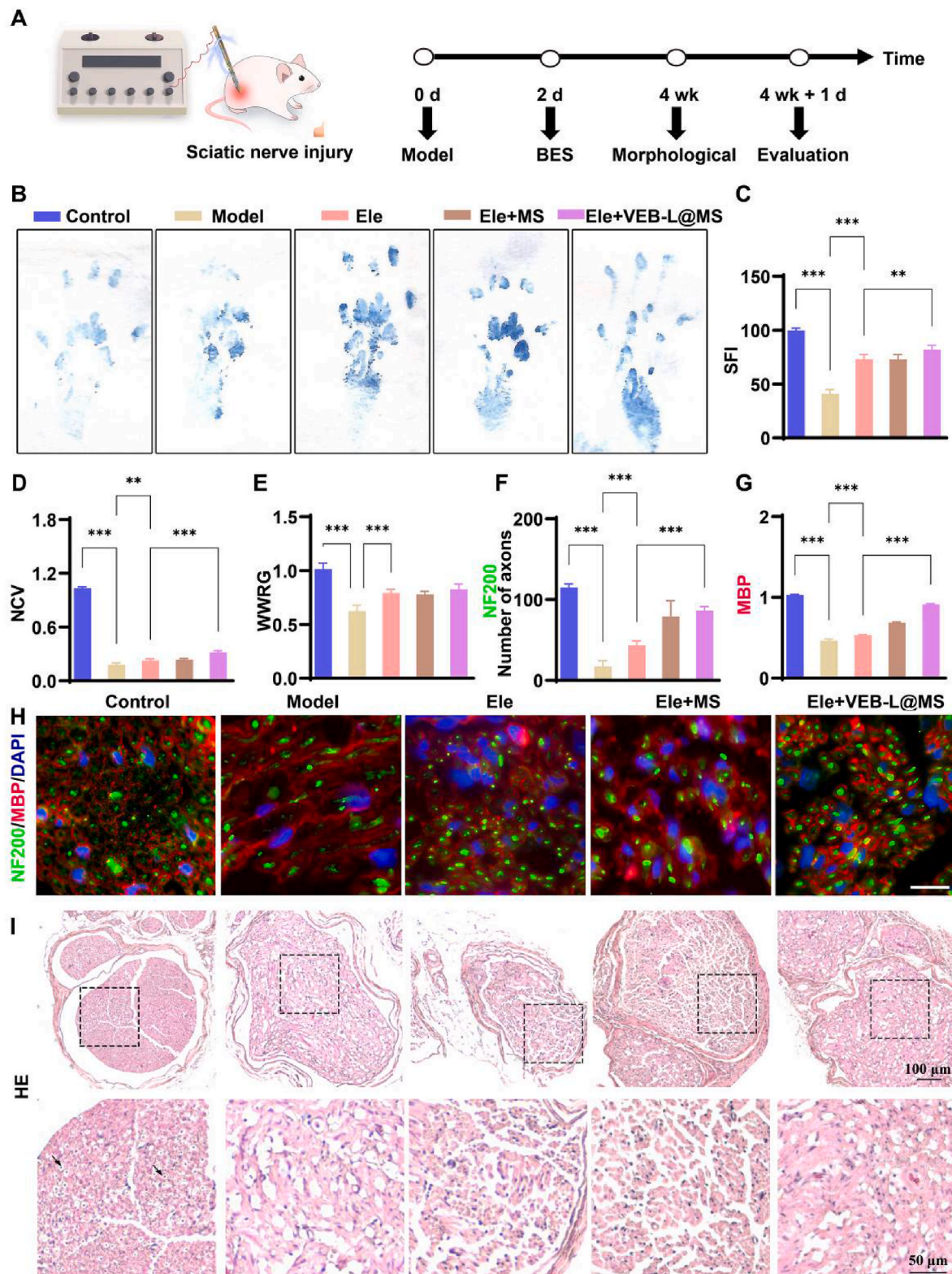


**Fig. 6.** The implementation of a threaded microneedle electrode system aids in promoting functional rehabilitation following sciatic nerve injury. (A) Schematic representation of animal experiments. (B, C) Footprint analysis to measure SFI. (D) NCV ratio determination (healthy side/damaged side). (E) Gastrocnemius muscle wet weight ratio measurement (healthy side/damaged side). (F) Statistical analysis of the number of axons in the injured nerve cross-section. (G) Statistical analysis of MBP average fluorescence density in the cross-section of the injured nerve. (H) Immunofluorescence staining of NF200 and MBP in the cross-section of the injured nerve (Bar = 20  $\mu$ m). (I) HE staining observation of nerve tissue (\*\* $P$  < 0.01, \*\*\* $P$  < 0.001, Bar = 100, 50  $\mu$ m).



secretion of a variety of chemical mediators) [92], and so on. Thus, this immunoreactivity may be part of the mechanism of action of needling. The threaded microneedles used in our experiments were consistent with acupuncture needles in terms of diameter and material, and we repeatedly adjusted the parameters to minimize the friction on the tissues during the early design and preparation process. Therefore, the immunoreactivity of threaded microneedles at the tissue interface should be similar to that of conventional acupuncture needles. In addition, we found differentially expressed reduced immune-related proteins (Fig. S16) by proteomic analysis of the local nerve tissue of electroacupuncture compared with the model group. Electroacupuncture is known to have bi-directional regulatory and anti-inflammatory repair effects after tissue injury. We hypothesized that electroacupuncture improves inflammation by decreasing these immune-related proteins to promote post-injury repair, which is consistent with what has been reported in the literature [93–95]. The regulation of rigid targeting of immune responses remains to be explored in greater depth.

### 3.6. Evaluation of microenvironment regulation by threaded microneedle electrode system

Building upon the confirmed enhancement of neuroregeneration by threaded microneedle electrode system in electrical stimulation therapy for nerve injuries, we investigated the microenvironment regulation by threaded microneedle electrode system. Schwann cells are crucial in myelin formation and facilitate nerve regeneration post-injury through the exchange of critical substances and information with axons, making them important regulatory cells in the neuroregenerative microenvironment [96]. S100 is an important marker for Schwann cell proliferation [97]. Immunofluorescence staining of Schwann cells showed that electrical stimulation increased S100 expression by 4.5 %, while combined stimulation with long microneedle electrodes significantly elevated S100 expression by 49.4 % (Fig. 7A and Fig. S17).

The expression of neurotrophic factors within the nervous system holds a pivotal role in nerve cell repair and survival. Following nerve injury, nerve growth factor (NGF) stimulates the growth of damaged neurons and supports synaptic reconstruction [98]. Brain-derived neurotrophic factor (BDNF) contributes positively to the survival, regeneration, and synaptic plasticity of neurons, thereby promoting neural connection restoration in affected areas. Additionally, glial cell-derived neurotrophic factor (GDNF) enhances neuronal axon growth and aids in neuronal function recovery [99]. Notably, electrical stimulation was observed to upregulate the expression of these three neurotrophic factors compared to the model group: NGF (79.4 %), BDNF (126.4 %), and GDNF (137.2 %). The threaded microneedle electrode system further elevated the expression levels of NGF (199.2 %), BDNF (164.7 %), and GDNF (189.7 %) compared to the model group (Fig. 7B–D). Given the significant regulatory roles of Schwann cells and neurotrophic factors in maintaining neuronal survival and promoting regeneration [100], the threaded microneedle electrode system has the potential to enhance the regenerative microenvironment.

We examined the tissue in the core region of electrical stimulation by proteomics and found that electrical stimulation elevated oxidative stress-related protein expression (Fig. S18). We found that the positive regulation-related proteins: C3 and Cfb, which are related to the clearance of apoptotic cells in the nerve tissue of the electrode area of the electroacupuncture group, were reduced compared with the model group by proteomic detection, which would be detrimental to the survival of the cells [101]. In addition, the pro-apoptotic protein CDK5 [102] was elevated, and the anti-apoptotic proteins Bclaf1 [103], DAD1 [104], UFL1 [105], and nicastrin [106] were reduced, suggesting that “electrical overload” in the core area could lead to cell damage (Fig. S19). The cell-killing effect of high-intensity electrical stimulation has been reported in the literature and applied to nano-knife treatment of tumors and other related diseases [107,108]. We evaluated the total

antioxidative capacity of neural tissues in the electrode area. We found that the threaded microneedle electrode system enhanced the tissue's total antioxidative capacity by 78.5 % compared to using electrical stimulation alone, indicating that threaded microneedle electrode system can significantly improve tissue antioxidative capacity (Fig. 6F). Post-injury, TUNEL staining revealed a heightened proportion of apoptotic cells within the nerve tissues (16.2 %). In the core region of electrical stimulation, the proportion of local apoptotic cells further increased (34.8 %). However, the threaded microneedle electrode system reduced cell apoptosis (4.3 %) (Fig. 7E). *In vivo* imaging demonstrated rapid drug release from the microspheres within 48 h, in line with the treatment frequency of once every other day, ensuring effective cell protection (Fig. 7G and H). In conclusion, these results indicate that the use of threaded microneedle electrode system for *in-situ* targeted delivery of microspheres significantly improves the regenerative microenvironment, counteracting cell damage from “electrical overload” in the core region of electrical stimulation, thereby promoting tissue repair. This provides a strategy to reduce the side effects of electrical stimulation therapy and enhance its effectiveness.

Currently, the development and application of nerve catheters can well enhance the repair of injured nerves [109,110], however, for most of the less severe nerve injuries, conservative treatment is generally the mainstay of treatment, and placement of catheters through surgery is not a priority. Electroacupuncture with an application of electrical stimulation after needling is widely used in clinical practice and has shown definite improvement in a wide range of disorders [111,112]. However, the effect of electroacupuncture on post-injury repair has its limitations, and further prolongation of time or elevation of current intensity on top of appropriate parameters may not necessarily lead to better results but rather may aggravate tissue fatigue and injury [113, 114]; On the other hand, electroacupuncture has a regulatory effect on multiple signaling pathways, the mechanisms of which are still being explored, and its regulation may be on the broad side and lack significance and specificity [115–117]. Therefore, we wished to mitigate the possible adverse effects of electrical stimulation in terms of its mode of action and initially achieved this with threaded microneedle electrodes.

## 4. Conclusion

This work developed a threaded microneedle electrode system for inhibiting the “electrical overload” in the core region of bioelectric stimulation, enhancing its therapeutic effectiveness. We utilized threaded long micro-needles as needle electrodes to load microspheres, achieving *in-situ* three-dimensional delivery of drugs to the electrically stimulated core region during bioelectric stimulation treatment. Liposomes containing VE succinate and VB12 were loaded into the microspheres. *In vitro* experiments confirmed that protective microspheres can alleviate bioelectric stimulation-induced oxidative stress and cell death. In *in vivo* experiments, we used the threaded microneedle electrode system as needle electrodes, achieving synchronized drug delivery at different depths of the three-dimensional structure in the core region of bioelectric stimulation. This reduces cell damage caused by “electrical overload” and improves the therapeutic effectiveness of bioelectric stimulation in repairing PNI. The main challenges in enhancing electrical stimulation therapy for nerve injury include uneven stimulation effects, and a lack of specificity in modulation. Our threaded microneedle electrode system has significantly improved the first challenge. To address the second, we will further explore and seek targeted modulating factors of electrical stimulation to enhance treatment efficacy. In conclusion, threaded microneedle electrode systems could effectively address the core region “electrical overload” problem during bioelectric stimulation treatment, providing insights to overcome the limitations of bioelectric stimulation therapy.

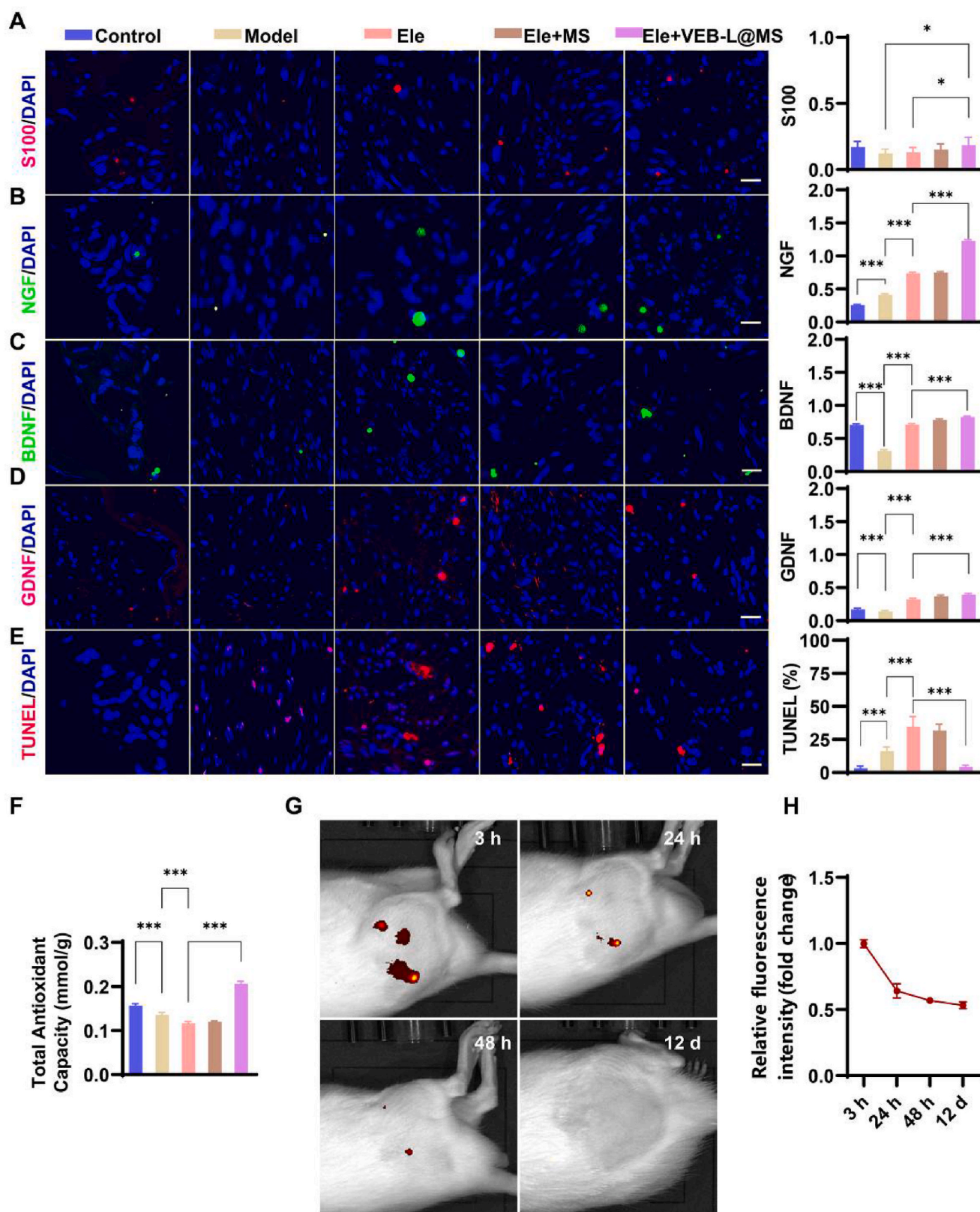


**Fig. 7.** The threaded microneedle electrode system improves the local regenerative microenvironment. (A) Immunofluorescence staining to detect S100 in the nerve slices of the injured nerve, reflecting Schwann cell proliferation and calculating average fluorescence density. (B–D) Immunofluorescence staining of NGF, BDNF, and GDNF in nerve sections and calculation of average fluorescence density to reflect the expression of neurotrophic factors. (E) TUNEL staining to detect cell apoptosis in locally electrically stimulated nerve tissue. (F) Total antioxidant capacity of the core area tissue of electrically stimulated injured sciatic nerves. (G, H) *In vivo* bioluminescence imaging to detect the *in-situ* delivery of fluorescent microspheres by long microneedles (\* $P < 0.05$ , \*\*\* $P < 0.001$ , Bar = 20  $\mu\text{m}$ ).

## CRediT authorship contribution statement

**Yupu Liu:** Writing – original draft, Methodology, Investigation, Data curation. **Yawei Du:** Writing – original draft, Methodology, Investigation. **Juan Wang:** Writing – review & editing, Methodology, Investigation. **Longxi Wu:** Investigation, Data curation. **Feng Lin:** Methodology, Data curation. **Wenguo Cui:** Writing – review & editing, Supervision, Project administration, Methodology, Investigation.

## Data availability statement

Upon request and subject to privacy and ethical considerations, the data that underlie the conclusions of this study can be accessed from the corresponding author. The data are not publicly accessible due to the necessity to uphold privacy and ethical standards.

## Ethics approval and consent to participate

All surgical and experimental procedures on rats were approved by the Animal Ethics Committee, Finock Biotechnology Co., LTD (AUP-20241227-01). All the authors were in compliance with all relevant ethical regulations.

## Declarations of competing interest

The authors declare that they have no known competing financial interests or personal relationships that could have appeared to influence the work reported in this paper.

## Acknowledgements

This research was financially supported by various grants, including the National Key Research and Development Program of China (2020YFA0908200), National Natural Science Foundation of China General Program (81930051, 82205244) and China Postdoctoral Science Foundation (2022M712135).

## Appendix A. Supplementary data

Supplementary data to this article can be found online at <https://doi.org/10.1016/j.bioactmat.2024.12.025>.

## References

- [1] K. Xu, X. Liu, X. Li, J. Yin, P. Wei, J. Qian, J. Sun, Effect of electrical and electromechanical stimulation on PC12 cell proliferation and axon outgrowth, *Front. Bioeng. Biotechnol.* (2021) 896.
- [2] S.J. Kim, R.R. Roy, H. Zhong, H. Suzuki, L. Ambartsumyan, F. Haddad, K. M. Baldwin, V.R. Edgerton, Electromechanical stimulation ameliorates inactivity-induced adaptations in the medial gastrocnemius of adult rats, *J. Appl. Physiol.* 103 (1) (2007) 195–205.
- [3] P. Kurz, G. Danner, J.P. Lembelembe, H.K. Nair, R. Martin, Activation of healing and reduction of pain by single-use automated microcurrent electrical stimulation therapy in patients with hard-to-heal wounds, *Int. Wound J.* (2023).
- [4] N.P. Aryan, H. Kaim, A. Rothermel, Primary current distribution and electrode geometry, in: N. Pour Aryan, H. Kaim, A. Rothermel (Eds.), *Stimulation and Recording Electrodes for Neural Prostheses*, Springer International Publishing, Cham, 2015, pp. 25–30.
- [5] L. He, W. He, Y. Wang, X. Wei, F. Du, G. Zhou, L.U. Zhang, S. Zhang, Neuromodulation model based on multi-electrode combined electrical stimulation and analysis of signal conduction mechanism, *J. Mech. Med. Biol.* 23 (2) (2023) 2350023.
- [6] J. Du, A. Morales, J. Paknahad, P. Kosta, J.C. Bouteiller, E. Fernandez, G. Lazzi, Electrode spacing and current distribution in electrical stimulation of peripheral nerve: a computational modeling study using realistic nerve models, in: 2021 43rd Annual International Conference of the IEEE Engineering in Medicine & Biology Society (EMBC), IEEE, 2021, pp. 4416–4419.
- [7] B. Sanchez, A. Pacheco, S.B. Rutkove, Guidelines to electrode positioning for human and animal electrical impedance myography research, *Sci. Rep.* 6 (1) (2016) 32615.
- [8] J. Wang, Q. Wang, Y. Fu, M. Lu, L. Chen, Z. Liu, X. Fu, X. Du, B. Yu, H. Lu, W. Cui, Swimming short fibrous nasal drops achieving intraventricular administration, *Sci. Bull.* 69 (9) (2024) 1249–1262.
- [9] A.E. Bergues Pupo, J.B. Reyes, L.E. Bergues Cabrales, J.M. Bergues Cabrales, Analytical and numerical solutions of the potential and electric field generated by different electrode arrays in a tumor tissue under electrotherapy, *Biomed. Eng. Online* 10 (1) (2011) 1–14.
- [10] E.R. Cosman Jr., E.R. Cosman Sr., Electric and thermal field effects in tissue around radiofrequency electrodes, *Pain Med.* 6 (6) (2005) 405–424.
- [11] J. Du, A. Morales, P. Kosta, J.C. Bouteiller, G. Martinez-Navarrete, D.J. Warren, E. Fernandez, G. Lazzi, Electrical stimulation induced current distribution in peripheral nerves varies significantly with the extent of nerve damage: a computational study utilizing convolutional neural network and realistic nerve models, *Int. J. Neural Syst.* 33 (4) (2023) 2350022.
- [12] K. Katoh, Effects of electrical stimulation of the cell: wound healing, cell proliferation, apoptosis, and signal transduction, *Med. Sci.* 11 (1) (2023) 11.
- [13] W. Yanagisawa, X.J. Wong, K. Haghighi, Irreversible electroporation (nanoknife) to unresectable pancreatic tumors: an initial Australian experience, *HPB* 24 (2022) S311–S312.
- [14] X. Wu, L. Xie, J. Lei, J. Yao, J. Li, L. Ruan, J. Hong, G. Zheng, Y. Cheng, L. Long, Acute traumatic coma awakening by right median nerve electrical stimulation: a randomised controlled trial, *Intensive Care Med.* (2023) 1–12.
- [15] F. Lin, Z. Wang, L. Xiang, L. Wu, Y. Liu, X. Xi, L. Deng, W. Cui, Transporting hydrogel via Chinese acupuncture needles for lesion positioning therapy, *Adv. Sci.* 9 (17) (2022) 2200079.
- [16] B. Zhang, R. Xie, J. Jiang, S. Hao, B. Fang, J. Zhang, H. Bai, B. Peng, L. Li, Z. Liu, Implantable neural electrodes: from preparation optimization to application, *J. Mater. Chem. C* (2023).
- [17] K. Shen, O. Chen, J.L. Edmunds, D.K. Piech, M.M. Maharbiz, Translational opportunities and challenges of invasive electrodes for neural interfaces, *Nat. Biomed. Eng.* 7 (4) (2023) 424–442.
- [18] S.T. Mahajan, M.P. Fitzgerald, K. Kenton, S. Shott, L. Brubaker, Concentric needle electrodes are superior to perineal surface-patch electrodes for electromyographic documentation of urethral sphincter relaxation during voiding, *BJU Int.* 97 (1) (2006) 117–120.
- [19] T. Yang, R. Cheng, J. Zhang, L. Tian, P. Sun, X. Ye, Effect of acupuncture treatment on post-stroke depression by using diamond-like ultra-thin nano-coating technology, *Cell. Mol. Biol.* 68 (3) (2022) 122–130.
- [20] F. Lin, Y. Zhuang, L. Xiang, T. Ye, Z. Wang, L. Wu, Y. Liu, L. Deng, W. Cui, Localization of lesion cells and targeted mitochondria via embedded hydrogel microsphere using heat transfer microneedles, *Adv. Funct. Mater.* (2023) 2212730.
- [21] F. Lin, Z. Wang, L. Xiang, L. Deng, W. Cui, Charge-guided micro/nano-hydrogel microsphere for penetrating cartilage matrix, *Adv. Funct. Mater.* 31 (49) (2021) 2107678.
- [22] F. Lin, L. Xiang, L. Wu, Y. Liu, Q. Jiang, L. Deng, W. Cui, Positioning regulation of organelle network via Chinese microneedle, *Sci. Adv.* 10 (16) (2024) 13063.
- [23] D.H. Lee, Y. Choi, M.H. Lee, J. Park, Comparison of tissue response and lifting effect induced by non-absorbable elastic thread and commercialized threads in rat model, *Regenerative Biomaterials* 11 (2024).
- [24] M. Sun, X. Wang, Y. Li, W. Yao, W. Gu, Mechanical effects of needle texture on acupoint tissue, *Journal of Integrative Medicine* 21 (3) (2023) 254–267.
- [25] C. Pan, J. Li, W. Hou, S. Lin, L. Wang, Y. Pang, Y. Wang, J. Liu, Polymerization-mediated multifunctionalization of living cells for enhanced cell-based therapy, *Adv. Mater.* 33 (13) (2021) 2007379.
- [26] B. Yi, L. Yu, H. Tang, W. Wang, W. Liu, Y. Zhang, Lysine-doped polydopamine coating enhances antithrombogenicity and endothelialization of an electrospun aligned fibrous vascular graft, *Appl. Mater. Today* 25 (2021) 101198.
- [27] J. Rao, C. Zhao, A. Zhang, H. Duan, P. Hao, R. Wei, J. Shang, W. Zhao, Z. Liu, J. Yu, K.S. Fan, Z. Tian, Q. He, W. Song, Z. Yang, Y.E. Sun, X. Li, NT3-chitosan enables de novo regeneration and functional recovery in monkeys after spinal cord injury, *Proc. Natl. Acad. Sci. USA* 115 (24) (2018) E5595–E5604.
- [28] H. Liu, Z. Cai, F. Wang, L. Hong, L. Deng, J. Zhong, Z. Wang, W. Cui, Colon-targeted adhesive hydrogel microsphere for regulation of gut immunity and flora, *Adv. Sci.* 8 (18) (2021) 2101619.
- [29] Y. Sun, H. Zhang, Y. Zhang, Z. Liu, D. He, W. Xu, S. Li, C. Zhang, Z. Zhang, Li–Mg–Si bioceramics provide a dynamic immuno-modulatory and repair-supportive microenvironment for peripheral nerve regeneration, *Bioact. Mater.* 28 (2023) 227–242.
- [30] B. Lopes, P. Sousa, R. Alvites, M. Branquinho, A.C. Sousa, C. Mendonça, L. M. Atayde, A.L. Luís, A.S. Varejão, A.C. Maurício, Peripheral nerve injury treatments and advances: one health perspective, *Int. J. Mol. Sci.* 23 (2) (2022) 918.
- [31] F. Fontana, A. Cafarelli, F. Iacoponi, S. Gasparini, T. Prateselli, A.N. Koppes, L. Ricotti, Pulsed electromagnetic field stimulation enhances neurite outgrowth in neural cells and modulates inflammation in macrophages, *Engineered Regeneration* 5 (1) (2024) 80–91.
- [32] G. Saulis, R. Rodaitė-Riševičienė, R. Saulė, Cytotoxicity of a cell culture medium treated with a high-voltage pulse using stainless steel electrodes and the role of iron ions, *Membranes* 12 (2) (2022) 184.
- [33] S. Yang, F. Wang, H. Han, H.A. Santos, Y. Zhang, H. Zhang, J. Wei, Z. Cai, Fabricated technology of biomedical micro-nano hydrogel, *Biomedical Technology* 2 (2023) 31–48.
- [34] S. Xu, Y. Liu, H. Lee, W. Li, Neural interfaces: bridging the brain to the world beyond healthcare, *Exploration* (2024) 20230146.



- [35] X. Shen, Z. Zhang, C. Cheng, C. Liu, N. Ma, D. Sun, D. Li, C. Wang, Bone regeneration and antibacterial properties of calcium-phosphorus coatings induced by gentamicin-loaded polydopamine on magnesium alloys, *Biomedical Technology* 5 (2024) 87–101.
- [36] W. Feng, Z. Wang, Shear-thinning and self-healing chitosan-graphene oxide hydrogel for hemostasis and wound healing, *Carbohydr. Polym.* 294 (2022) 119824.
- [37] A.K. Petrus, A.R. Vortherms, T.J. Fairchild, R.P. Doyle, Vitamin B12 as a carrier for the oral delivery of insulin, *ChemMedChem* 2 (12) (2007) 1717–1721.
- [38] J.F. McEwan, H.S. Veitch, G.J. Russell-Jones, Synthesis and biological activity of ribose-5'-carbamate derivatives of vitamin B12, *Bioconjugate Chem.* 10 (6) (1999) 1131–1136.
- [39] W. Xiong, Z. Han, S. Ding, H. Wang, Y. Du, W. Cui, M. Zhang, In situ remodeling of efferocytosis via lesion-localized microspheres to reverse cartilage senescence, *Adv. Sci.* n/a (n/a) (2024) 2400345.
- [40] Y. Du, Z. Wang, T. Wang, W. He, W. Zhou, M. Li, C. Yao, X. Li, Improved antitumor activity of novel redox-responsive paclitaxel-encapsulated liposomes based on disulfide phosphatidylcholine, *Mol. Pharm.* 17 (1) (2019) 262–273.
- [41] Y. Du, C. Li, Y. Zhang, W. Xiong, F. Wang, J. Wang, Y. Zhang, L. Deng, X. Li, W. Chen, In situ-activated phospholipid-mimic artemisinin prodrug via injectable hydrogel nano/microsphere for rheumatoid arthritis therapy, *Research* 2022 (2022) 3.
- [42] Schelling Birgit, Toledo Mettler, Using UV/VIS spectroscopy for different types of vitamin B12 analysis, *Int. labmate* 43 (1) (2018) 24.
- [43] F. Gamna, S. Spriano, Vitamin E: a review of its application and methods of detection when combined with implant biomaterials, *Materials* 14 (13) (2021).
- [44] Y. Lei, Y. Wang, J. Shen, Z. Cai, Y. Zeng, P. Zhao, J. Liao, C. Lian, N. Hu, X. Luo, Stem cell-recruiting injectable microgels for repairing osteoarthritis, *Adv. Funct. Mater.* 31 (48) (2021) 2105084.
- [45] Y. He, M. Sun, J. Wang, X. Yang, C. Lin, L. Ge, C. Ying, K. Xu, A. Liu, L. Wu, Chondroitin sulfate microspheres anchored with drug-loaded liposomes play a dual antioxidant role in the treatment of osteoarthritis, *Acta Biomater.* 151 (2022) 512–527.
- [46] Y. Li, J. Zheng, Y. Zhu, Y. Qu, R. Suo, Y. Zhu, Neuroprotective effects of methylcobalamin in cerebral ischemia/reperfusion injury through activation of the ERK1/2 signaling pathway, *Int. Immunopharm.* 99 (2021) 108040.
- [47] W.S. Cheow, K. Hadinoto, Factors affecting drug encapsulation and stability of lipid-polymer hybrid nanoparticles, *Colloids Surf. B Biointerfaces* 85 (2) (2011) 214–220.
- [48] G. Napolitano, G. Fasciolo, S. Di Meo, P. Venditti, Vitamin E supplementation and mitochondria in experimental and functional hyperthyroidism: a mini-review, *Nutrients* 11 (12) (2019) 2900.
- [49] Y. Gao, Q. Ma, Bacterial infection microenvironment-responsive porous microspheres by microfluidics for promoting anti-infective therapy, *Smart Medicine* 1 (1) (2022) e20220012.
- [50] Z. Chen, Z. Lv, Y. Zhuang, Q. Saiding, W. Yang, W. Xiong, Z. Zhang, H. Chen, W. Cui, Y. Zhang, Mechanical signal-tailored hydrogel microspheres recruit and train stem cells for precise differentiation, *Adv. Mater.* (2023) 2300180.
- [51] H. Chen, H. Xue, H. Zeng, M. Dai, C. Tang, L. Liu, 3D printed scaffolds based on hyaluronic acid bioinks for tissue engineering: a review, *Biomater. Res.* 27 (1) (2023) 137.
- [52] N. Yang, C. Sun, C. Dong, Y. Huang, Y. Zhu, Z. Gu, Emerging microfluidics for the modeling and treatment of arthritis, *Engineered Regeneration* 5 (2) (2024) 153–169.
- [53] Z. Chen, Z. Lv, Z. Zhang, Y. Zhang, W. Cui, Biomaterials for microfluidic technology, *Materials Futures* 1 (1) (2022) 12401.
- [54] X. Liu, Y. Zhuang, W. Huang, Z. Wu, Y. Chen, Q. Shan, Y. Zhang, Z. Wu, X. Ding, Z. Qiu, W. Cui, Z. Wang, Interventional hydrogel microsphere vaccine as an immune amplifier for activated antitumor immunity after ablation therapy, *Nat. Commun.* 14 (1) (2023) 4106.
- [55] A.C. Daly, L. Riley, T. Segura, J.A. Burdick, Hydrogel microparticles for biomedical applications, *Nat. Rev. Mater.* 5 (1) (2020) 20–43.
- [56] Y. Zhuang, W. Cui, Biomaterial-based delivery of nucleic acids for tissue regeneration, *Adv. Drug Deliv. Rev.* 176 (2021) 113885.
- [57] P. Xiao, X. Han, Y. Huang, J. Yang, L. Chen, Z. Cai, N. Hu, W. Cui, W. Huang, Reprogramming macrophages via immune cell mobilized hydrogel microspheres for osteoarthritis treatments, *Bioact. Mater.* 32 (2024) 242–259.
- [58] X. Li, X. Li, J. Yang, Y. Du, L. Chen, G. Zhao, T. Ye, Y. Zhu, X. Xu, L. Deng, In situ sustained macrophage-targeted nanomicelle-hydrogel microspheres for inhibiting osteoarthritis, *Research* 6 (2023) 131.
- [59] Z. Zhao, Z. Wang, G. Li, Z. Cai, J. Wu, L. Wang, L. Deng, M. Cai, W. Cui, Injectable microfluidic hydrogel microspheres for cell and drug delivery, *Adv. Funct. Mater.* 31 (31) (2021) 2103339.
- [60] J. Shen, A. Chen, Z. Cai, Z. Chen, R. Cao, Z. Liu, Y. Li, J. Hao, Exhausted local lactate accumulation via injectable nanozyme-functionalized hydrogel microsphere for inflammation relief and tissue regeneration, *Bioact. Mater.* 12 (2022) 153–168.
- [61] X. Chen, L. Ren, H. Zhang, Y. Hu, M. Liao, Y. Shen, K. Wang, J. Cai, H. Cheng, J. Guo, Y. Qi, H. Wei, X. Li, L. Shang, J. Xiao, J. Sun, R. Chai, Basic fibroblast growth factor-loaded methacrylate gelatin hydrogel microspheres for spinal nerve regeneration, *Smart Medicine* 2 (2) (2023) e20220038.
- [62] Y. Liu, Y. Yang, F. Mou, J. Zhu, H. Li, T. Zhao, Y. Zhao, S. Shao, G. Cui, H. Guo, Exosome-mediated miR-21 was involved in the promotion of structural and functional recovery effect produced by electroacupuncture in sciatic nerve injury, *Oxidative Med. Cell. Longev.* 2022 (2022).
- [63] D. Guo, Q. An, Z. Xiao, S. Zhai, D. Yang, Efficient removal of Pb(II), Cr(VI) and organic dyes by polydopamine modified chitosan aerogels, *Carbohydr. Polym.* 202 (2018) 306–314.
- [64] Y. Wang, Y. Zhao, M. Li, S. Shi, Y. Gong, Fabrication of antifouling-antibacterial dual functional polymer coating via dopamine-based multiple interactions, *Chem. J. Chin. Univ.* 42 (3) (2021) 811–818.
- [65] G. Wu, X. Wen, R. Kuang, K.W. Lui, B. He, G. Li, Z. Zhu, Roles of macrophages and their interactions with Schwann cells after peripheral nerve injury, *Cell. Mol. Neurobiol.* 44 (1) (2023) 11.
- [66] S. Bolívar, X. Navarro, E. Udina, Schwann cell role in selectivity of nerve regeneration, *Cells* 9 (9) (2020).
- [67] Y. Guan, Z. Ren, B. Yang, W. Xu, W. Wu, X. Li, T. Zhang, D. Li, S. Chen, J. Bai, X. Song, Z. Jia, X. Xiong, S. He, C. Li, F. Meng, T. Wu, J. Zhang, X. Liu, H. Meng, J. Peng, Y. Wang, Dual-bionic regenerative microenvironment for peripheral nerve repair, *Bioact. Mater.* 26 (2023) 370–386.
- [68] M. Bosch-Queralt, R. Fledrich, R.M. Stassart, Schwann cell functions in peripheral nerve development and repair, *Neurobiol. Dis.* 176 (2023) 105952.
- [69] R.M. Stassart, J.A. Gomez-Sanchez, A.C. Lloyd, Schwann cells as orchestrators of nerve repair: implications for tissue regeneration and pathologies, *Cold Spring Harbor Perspect. Biol.* 16 (6) (2024) a41363.
- [70] J. Li, R. Guan, L. Pan, Mechanism of Schwann cells in diabetic peripheral neuropathy: a review, *Medicine (Baltim.)* 102 (1) (2023) e32653.
- [71] Y. Zou, S. Wu, Q. Hu, H. Zhou, Y. Ge, Z. Ju, S. Luo, Sonic hedgehog restrains the ubiquitin-dependent degradation of SP1 to inhibit neuronal/glia senescence associated phenotypes in chemotherapy-induced peripheral neuropathy via the TRIM25-CXCL13 axis, *J. Adv. Res.* (2024).
- [72] X. Wang, W. Yang, L. Wang, L. Zheng, W.S. Choi, Platinum-based chemotherapy induces demyelination of Schwann cells in oral squamous cell carcinoma treatment, *Toxicol. Appl. Pharmacol.* 481 (2023) 116751.
- [73] E.B. Evans, S.W. Brady, A. Tripathi, D. Hoffman-Kim, Schwann cell durotaxis can be guided by physiologically relevant stiffness gradients, *Biomater. Res.* 22 (1) (2018) 14.
- [74] D. Xu, H. Zhang, Y. Wang, Y. Zhang, F. Ye, L. Lu, R. Chai, Piezoelectric biomaterials for neural tissue engineering, *Smart Medicine* 2 (2) (2023) e20230002.
- [75] H. Dong, H. Wu, Y. Tang, Y. Huang, R. Lin, J. Zhao, X. Xu, AMPK regulates mitochondrial oxidative stress in C2C12 myotubes induced by electrical stimulations of different intensities, *Nan Fang yi ke da xue xue bao = Journal of Southern Medical University* 38 (6) (2018) 742–747.
- [76] H. Dong, H. Wu, Z. Tian, Z. Luo, Y. Wu, J. Zhao, Electrical stimulation induces mitochondrial autophagy via activating oxidative stress and Sirt3 signaling pathway, *Chin. Med. J.* 134 (5) (2021).
- [77] W. Derave, N. Straumann, R.A. Olek, P. Hespel, Electrolysis stimulates creatine transport and transporter cell surface expression in incubated mouse skeletal muscle: potential role of ROS, *Am. J. Physiol.-Endocrinol. Metab.* 291 (6) (2006) E1250–E1257.
- [78] X. Fu, J. Wang, D. Qian, L. Xi, L. Chen, Y. Du, W. Cui, Y. Wang, Oxygen atom-concentrating short fibrous sponge regulates cellular respiration for wound healing, *Adv. Fiber Mater.* 5 (5) (2023) 1773–1787.
- [79] Z. Su, Z. Li, R. Zhang, H. Xie, Y. Deng, B.Z. Tang, Simulated microgravity-induced endogenous H2O2 traced by an AIEgen, *Sci. Bull.* 67 (24) (2022) 2513–2516.
- [80] M.H. Lee, Y.J. Park, S.H. Hong, M. Koo, M. Cho, J. Park, Pulsed electrical stimulation enhances consistency of directional migration of adipose-derived stem cells, *Cells* 10 (11) (2021) 2846.
- [81] W. Jing, Y. Zhang, Q. Cai, G. Chen, L. Wang, X. Yang, W. Zhong, Study of electrical stimulation with different electric-field intensities in the regulation of the differentiation of PC12 cells, *ACS Chem. Neurosci.* 10 (1) (2019) 348–357.
- [82] T. Chung, Y. Hsu, T. Chen, Y. Li, H. Yang, J. Yu, I. Lee, P. Lai, Y.E. Li, P. Chen, Machine learning integrated workflow for predicting Schwann cell viability on conductive MXene biointerfaces, *ACS Appl. Mater. Interfaces* 15 (39) (2023) 46460–46469.
- [83] Y. Wang, J. Guo, X. Cao, Y. Zhao, Developing conductive hydrogels for biomedical applications, *Smart Medicine* 3 (1) (2024) e20230023.
- [84] P. Bian, J. Zhang, J. Wang, J. Yang, J. Wang, H. Liu, Y. Sun, M. Li, X. Zhang, Enhanced catalysis of ultrasmall Au-MoS<sub>2</sub> clusters against reactive oxygen species for radiation protection, *Sci. Bull.* 63 (14) (2018) 925–934.
- [85] T. Li, H. Wang, H. Zhang, P. Zhang, M. Zhang, H. Feng, X. Duan, W. Liu, X. Wang, Z. Sun, Effect of breathing exercises on oxidative stress biomarkers in humans: a systematic review and meta-analysis, *Front. Med.* 10 (2023) 1121036.
- [86] M. Bervar, Video analysis of standing — an alternative footprint analysis to assess functional loss following injury to the rat sciatic nerve, *J. Neurosci. Methods* 102 (2) (2000) 109–116.
- [87] D. Umansky, K.M. Hagen, T.H. Chu, R.K. Pathiyil, S. Alzahrani, S.S. Ousman, R. Midha, Functional gait assessment using manual, semi-automated and deep learning approaches following standardized models of peripheral nerve injury in mice, *Biomolecules* 12 (10) (2022) 1355.
- [88] X. Li, T. Zhang, C. Li, W. Xu, Y. Guan, X. Li, H. Cheng, S. Chen, B. Yang, Y. Liu, Electrical stimulation accelerates Wallerian degeneration and promotes nerve regeneration after sciatic nerve injury, *Glia* 71 (3) (2023) 758–774.
- [89] Y. Qian, Z. Yan, T. Ye, V. Shahin, J. Jiang, C. Fan, Decoding the regulatory role of ATP synthase inhibitory factor 1 (ATP1F1) in Wallerian degeneration and peripheral nerve regeneration, *Exploration* (2024) 20230098.
- [90] M. Wang, W. Liu, J. Ge, S. Liu, The immunomodulatory mechanisms for acupuncture practice, *Front. Immunol.* 14 (2023) 1147718.

- [91] W. Yu, J. Park, H. Park, S. Kim, Changes of local microenvironment and systemic immunity after acupuncture stimulation during inflammation: a literature review of animal studies, *Front. Neurol.* 13 (2023) 1086195.
- [92] S.S. Ding, S.H. Hong, C. Wang, Y. Guo, Z.K. Wang, Y. Xu, Acupuncture modulates the neuro-endocrine-immune network, *QJM: An International Journal of Medicine* 107 (5) (2013) 341–345.
- [93] S. Liu, Z. Wang, Y. Su, L. Qi, W. Yang, M. Fu, X. Jing, Y. Wang, Q. Ma, A neuroanatomical basis for electroacupuncture to drive the vagal-adrenal axis, *Nature* 598 (7882) (2021) 641–645.
- [94] Y. Chen, M. Cai, B. Shen, C. Fan, X. Zhou, Electroacupuncture at Zusanli regulates the pathological phenotype of inflammatory bowel disease by modulating the NLRP3 inflammasome pathway, *Immunity, Inflammation and Disease* 12 (8) (2024) e1366.
- [95] A.Y. Fan, Anti-inflammatory mechanism of electroacupuncture involves the modulation of multiple systems, levels and targets and is not limited to “driving the vagus-adrenal axis”, *Journal of Integrative Medicine* 21 (4) (2023) 320–323.
- [96] J.T. Oliveira, C. Yanick, N. Wein, L.C. Gomez, Neuron-Schwann cell interactions in peripheral nervous system homeostasis, disease, and preclinical treatment, *Front. Cell. Neurosci.* 17 (2023) 1248922.
- [97] R. Deng, Z. Luo, Z. Rao, Z. Lin, S. Chen, J. Zhou, Q. Zhu, X. Liu, Y. Bai, D. Quan, Decellularized extracellular matrix containing electrospun fibers for nerve regeneration: a comparison between core-shell structured and preblended composites, *Adv. Fiber Mater.* 4 (3) (2022) 503–519.
- [98] Y. Ikegami, M. Shafiq, S. Aishima, H. Ijima, Heparin/growth factors-immobilized aligned electrospun nanofibers promote nerve regeneration in polycaprolactone/gelatin-based nerve guidance conduits, *Adv. Fiber Mater.* 5 (2) (2023) 554–573.
- [99] A. Asgari Taei, L. Dargahi, P. Khodabakhsh, M. Kadivar, M. Farahmandfar, Hippocampal neuroprotection mediated by secretome of human mesenchymal stem cells against experimental stroke, *CNS Neurosci. Therapy* 28 (9) (2022) 1425–1438.
- [100] W.M. Stansberry, B.A. Pierchala, Neurotrophic factors in the physiology of motor neurons and their role in the pathobiology and therapeutic approach to amyotrophic lateral sclerosis, *Front. Molec. Neurosciences* 16 (2023) 1238453.
- [101] S.K. Sahu, Intracellular complement protein C3 promotes cell survival via Factor B (FB), *J. Immunol.* 210 (1 Supplement) (2023) 71–79.
- [102] S. Liu, Correlation between caspase-1, Cdk5, NLRP3 and idiopathic inflammatory myopathy, *Adv. Clin. Med.* 13 (2023) 9599–9604.
- [103] A. Shao, Y. Lang, M. Wang, C. Qin, Y. Kuang, Y. Mei, D. Lin, S. Zhang, J. Tang, Bclaf1 is a direct target of HIF-1 and critically regulates the stability of HIF-1 $\alpha$  under hypoxia, *Oncogene* 39 (13) (2020) 2807–2818.
- [104] N.A. Hong, N.H. Kabra, S.N. Hsieh, D. Cado, A. Winoto, In vivo overexpression of Dad1, the defender against apoptotic death-1, enhances T cell proliferation but does not protect against apoptosis, *J. Immunol.* 163 (4) (1999) 1888–1893.
- [105] J. Li, X. Tang, X. Tu, Z. Jin, H. Dong, Q. Yang, T. Yao, Z. Pan, UFL1 alleviates ER stress and apoptosis stimulated by LPS via blocking the ferroptosis pathway in human granulosa-like cells, *Cell Stress & Chaperones* 27 (5) (2022) 485–497.
- [106] X. Wang, X. Wang, Y. Xu, M. Yan, W. Li, J. Chen, T. Chen, Effect of nicastrin on hepatocellular carcinoma proliferation and apoptosis through PI3K/AKT signalling pathway modulation, *Cancer Cell Int.* 20 (1) (2020) 91.
- [107] D. Martín, D. Ruano, A. Yúfera, P. Daza, Electrical pulse stimulation parameters modulate N2a neuronal differentiation, *Cell Death Dis.* 10 (1) (2024) 49.
- [108] C. Chen, X. Bai, Y. Ding, I. Lee, Electrical stimulation as a novel tool for regulating cell behavior in tissue engineering, *Biomater. Res.* 23 (1) (2019) 25.
- [109] D. Xu, S. Fu, H. Zhang, W. Lu, J. Xie, J. Li, H. Wang, Y. Zhao, R. Chai, Ultrasound-Responsive aligned piezoelectric nanofibers derived hydrogel conduits for peripheral nerve regeneration, *Adv. Mater.* 36 (28) (2024) e2307896.
- [110] C. Hu, B. Liu, X. Huang, Z. Wang, K. Qin, L. Sun, Z. Fan, Sea cucumber-inspired microneedle nerve guidance conduit for synergistically inhibiting muscle atrophy and promoting nerve regeneration, *ACS Nano* 18 (22) (2024) 14427–14440.
- [111] C. Wang, Y. Liu, L. Li, H. Zhang, Z. Ye, L. Zhao, The efficacy of electroacupuncture for cervical nerve edema and movement disorder caused by the brachial plexus injury: a case report, *Front. Neurol.* 15 (2024) 1342844.
- [112] M.Y. Tian, Y.D. Yang, W.T. Qin, B.N. Liu, F.F. Mou, J. Zhu, H.D. Guo, S.J. Shao, Electroacupuncture promotes nerve regeneration and functional recovery through regulating lncRNA GAS5 targeting miR-21 after sciatic nerve injury, *Mol. Neurobiol.* 61 (2) (2024) 935–949.
- [113] R. Zhang, L. Lao, K. Ren, B.M. Berman, Mechanisms of acupuncture-electroacupuncture on persistent pain, *Anesthesiology* 120 (2) (2014) 482–503.
- [114] Y. Liang, J. Zhou, J. Sun, X. Fan, S. Zheng, J. Fang, J. Fang, The dose-effect relationship of electroacupuncture analgesia and its stimulus parameters: progress in the last 3 decades, *World J. Acupuncture-Moxibustion* 33 (1) (2023) 12–19.
- [115] H. Lee, J. Lee, D. Jung, H. Oh, H. Shin, B. Choi, Neuroprotection of transcranial cortical and peripheral somatosensory electrical stimulation by modulating a common neuronal death pathway in mice with ischemic stroke, *Int. J. Mol. Sci.* 25 (14) (2024).
- [116] R. Wu, H. Ma, J. Hu, D. Wang, F. Wang, X. Yu, Y. Li, W. Fu, M. Lai, Z. Hu, W. Feng, C. Shan, C. Wang, Electroacupuncture stimulation to modulate neural oscillations in promoting neurological rehabilitation, *Brain Res.* 1822 (2024) 148642.
- [117] M. Zhou, Q. Zhang, M. Huo, H. Song, H. Chang, J. Cao, Y. Fang, D. Zhang, The mechanistic basis for the effects of electroacupuncture on neuropathic pain within the central nervous system, *Biomed. Pharmacother.* 161 (2023) 114516.